PONTIFICIA UNIVERSIDAD CATOLICA DE CHILE

ESCUELA DE INGENIERIA

AN INVESTIGATION OF THE COUPLED WATER AND HEAT TRANSPORT IN GREEN ROOF SUBSTRATES

VICTORIA P. SANDOVAL VALDÉS

Thesis submitted to the Office of Research and Graduate Studies in partial fulfillment of the requirements for the Degree of Master of Science in Engineering

Advisor:

FRANCISCO SUÁREZ POCH

Santiago de Chile, (December, 2016)

© 2016, Victoria Sandoval

PONTIFICIA UNIVERSIDAD CATOLICA DE CHILE
ESCUELA DE INGENIERIA

AN INVESTIGATION OF THE COUPLED WATER AND HEAT TRANSPORT IN GREEN ROOF SUBSTRATES

VICTORIA PAZ SANDOVAL VALDÉS

Members of the Committee:

FRANCISCO SUÁREZ POCH

CARLOS BONILLA MELÉNDEZ

MARÍA FERNANDA HERNÁNDEZ LÓPEZ

CHRISTIAN DANI GUZMÁN

Thesis submitted to the Office of Research and Graduate Studies in partial fulfillment of the requirements for the Degree of Master of Science in Engineering

Santiago de Chile, (December, 2016)

ACKNOWLEDGEMENTS

First and foremost, I have to thank my advisor, Dr. Francisco Suárez for his concern and constant encouragement during the investigation.

I want to thank to whole team of the Department of Hydraulic and Environmental Engineering, especially to my friends Vasty, Guillermo, Lorena, Pablo, Maximiliano, Francisca, Mauricio and Alex, for their friendship, support and patience during my stay in the office. I also thank my friends of the School of Engineering for their company and great moments during the career.

I also thank the support of from the Center for Sustainable Urban Development (CEDEUS - CONICYT/FONDAP/15110020). I also want thank other projects that partially funded this work (INNOVA-CORFO 12IDL2-13630, CONICYT/FONDECYT/1131131). Likewise want to thank the people who helped in this investigation, Nicole, Macarena, Coté, José and Eduardo.

I am indeed grateful to my parents and sisters, who are always a source of support and affection.

The most special thanks goes to my boyfriend Marcos support and encourage my investigation.

CONTENTS

Page

LIST OF TABLES

Page

LIST OF FIGURES

Page

RESUMEN

Las cubiertas vegetales integran vegetación a los edificios, minimizando los requerimientos energéticos y escorrentía superficial. Para optimizar estos beneficios, se necesita un entendimiento de los procesos que controlan los flujos de agua y calor en cubiertas vegetales. Los factores principales que determinan los flujos de agua y calor en las cubiertas vegetales son las características hidrodinámicas y térmicas de las capas de sustrato y vegetación. Los sustratos son medios porosos artificiales que se usan para objetivos tecnológicos e ingenieriles. La compactación de un sustrato afecta los procesos físicos que ocurren en el mismo y no se ha estudiado su efecto en los flujos de calor y agua. En este estudio se han caracterizado las propiedades físicas, hidrodinámicas y térmicas de cinco sustratos de cubiertas vegetales. Además, se evaluó el efecto de la compactación en estas propiedades realizando un ajuste teórico a los parámetros térmicos e hidráulicos obtenidos anteriormente. Se realizaron simulaciones numéricas de flujos de agua y calor acoplados para evaluar el impacto de las propiedades obtenidas y compactadas en el comportamiento hidráulico y térmico de un sistema de una cubierta vegetal. Los cinco sustratos mostraron gran capacidad de almacenar y transportar flujos de agua, mientras que su capacidad de transportar calor fue similar a otros sustratos de cubiertas vegetales reportados en la literatura. Bajo condiciones no saturadas, la capacidad de retención y el volumen de almacenamiento de los sustratos controlaron la respuesta hidráulica de cada sustrato. El efecto de la compactación muestra la disminución de espacio de poros y el aumento de fuerzas capilares, provocando una reducción del volumen de almacenamiento. En las propiedades térmicas se observa un incremento general de la conductividad dado el aumento de contacto entre partículas. Las simulaciones numéricas muestran que el sustrato de tierra de hoja con perlita presenta la menor difusión vertical de calor y una alta capacidad para almacenar agua (mismo resultado obtenido cuando los sustratos se compactan). La modelación dinámica presentada en este estudio puede representar la complejidad de los procesos que ocurren en las cubiertas vegetales y puede ser una herramienta útil para diseñar la configuración de una cubierta vegetal.

ABSTRACT

Green roofs integrate vegetation into buildings thereby minimizing energy requirements and water runoff. An understanding of the processes controlling water and heat fluxes in green roofs under site-specific climatic conditions is needed to optimize their benefits. The hydrodynamic and thermal characteristics of substrates and vegetation layers are the primary controlling factors determining water and heat fluxes on green roofs. Substrates are artificial porous media that are used for engineering and technological purposes. Soil compaction affects the water physical processes that occur within green roof substrates and this process has not been taken into account in water and heat fluxes. In this study, I characterized the physical, hydrodynamic and thermal properties of five green roof substrates. Additionally, the evaluation of substrates compaction was performed through a theoretical adjustment on the previous thermal and hydraulic parameters. I performed coupled heat and water transport numerical simulations to assess the impact of the previous properties on the hydraulic and thermal performance of a hypothetical roof system. The five substrates showed a large capacity to store and transport water, while their ability to conduct heat was similar to other green roof substrates reported in the literature. Under unsaturated conditions, the water retention and the storage capacity of the substrates controlled the hydraulic response of each substrate. The effect of compaction in water properties shows the decrease of pore size and the increment of capillary forces, causing a reduction of volume storage. The thermal properties show an increasing trend in the thermal conductivity due to the increment of particle contact. Our simulations results show that the substrate with peat and perlite is the one with the best capacity to store water and to reduce the heat flux trough the substrate layer (even when the substrates are compacted). This substrate outperforms the others most likely due to its low thermal conductivity and its large pore space. The dynamic modeling presented in this study can represent the complexity of the processes that are occurring in green roof substrates and thus, it is a tool that can be used to design the configuration of a green roof.

1 INTRODUCTION

1.1 Motivation

Green roofs have become widely adopted over the past 20 years as a technological response to a wide public concern towards sustainable development, controlling greenhouse gas emissions and increasing energy efficiency (Hashemi et al., 2015). They integrate vegetation into buildings, with the aim of minimizing some of the negative impacts of urbanizations (Raji et al., 2015). A properly designed green roof can decrease environmental pollution, noise levels, building energy consumption, and stormwater runoff (Vijayaraghavan, 2016), while they provide ecological services and increase urban biodiversity (Brown and Lundholm, 2015).

The overall performance of green roofs depends on the interaction between environmental conditions and the biophysical components of green roofs (Raji et al., 2015). The appropriate selection of its components is key to develop a green roof that can optimize the response under site-specific climate conditions and local materials (Vijayaraghavan, 2016). The substrate and the vegetation layers are the most important components determining water and heat fluxes on green roofs (Buckland-Nicks et al., 2016). In this investigation, without detracting the important role that vegetation has on the hydraulic and thermal performance of a green roof, I focused on green roof substrates. The substrate is an engineered media that has an improved performance compared to natural soils (Brown and Lundholm, 2015). It provides critical resources for the vegetation: water, nutrients, and a support media (Campbell and Norman, 2013). The water retention capacity and the thermal behavior of a green roof strongly depend on the physical properties of the substrate (Campbell and Norman, 2013). The moisture content of the substrate it is a key element for vegetation survival, especially in arid and semi-arid climates. In addition, substrate compaction modifies the structure of the porous medium, changing the moisture evolution and the response of the green roof to the atmospheric conditions (Alaoui et al., 2011). Hence, to improve the overall performance of green roofs, it is important to characterize the physical, hydrodynamic and thermal properties of green roof substrates.

1.2 Objectives

The general objective of this work is to investigate how the hydrodynamic and thermal properties of substrates influence the water and heat transport in green roof substrates considering all the water flow mechanisms found in green roofs. The specific objectives are: 1) to characterize a set of five organic and mineral green roof substrates in terms of their hydrodynamic and thermal properties: water retention curve, hydraulic conductivity curve, thermal conductivity, and specific heat capacity; 2) to evaluate the impacts of the previous properties on the water and heat transport through green roof substrates using numerical simulations; 3) to develop a methodology based on theoretical considerations combined with empirical information that can be used to represent the effect of compaction on the hydrodynamic and thermal properties of a porous medium, and 4) to predict water and heat fluxes to the compacted green roof substrates with the use of numerical simulations.

1.3 Structure of the thesis

This thesis is organized in the following way. Chapter 1 is a brief introduction to the topic that shows the motivation of this work, and the general and specific objectives of the thesis. Chapter 2 corresponds to a manuscript entitled “Porous media characterization to simulate water and heat transport through green roof substrates” that is currently under review in a peer-review journal. Chapter 3 is a manuscript called “A new method to determine how compaction affects water and heat transport in porous media – application to green roof substrates” that will be submitted for peer-review. Finally, chapter 4 corresponds to the conclusions and perspectives that can be drawn from the work reported in chapters 2 and 3.

2 POROUS MEDIA CHARACTERIZATION TO SIMULATE WATER AND HEAT TRANSPORT THROUGH GREEN ROOF SUBSTRATES

2.1 Abstract

Green roofs integrate vegetation into buildings thereby minimizing energy requirements and water runoff. An understanding of the processes controlling water and heat fluxes in green roofs under site-specific climatic conditions is needed to optimize their benefits. The hydrodynamic and thermal characteristics of substrates and vegetation layers are the primary controlling factors determining water and heat fluxes on green roofs. In this study, I characterized the physical, hydrodynamic and thermal properties of five green roof substrates (S1-S5). I performed coupled heat and water transport numerical simulations to assess the impact of the previous properties on the hydraulic and thermal performance of a hypothetical roof system. The five substrates showed a large capacity to store and transport water, while their ability to conduct heat was similar to other green roof substrates reported in the literature. Under unsaturated conditions, the water retention and the storage capacity of the substrates controlled the hydraulic response of each substrate. Our simulations results show that the S2 substrate is the one with the best capacity to store water and to reduce the heat flux trough the substrate layer. This substrate outperforms the others most likely due to its low thermal conductivity and its large pore space. The dynamic modeling presented in this study can represent the complexity of the processes that are occurring in green roof substrates and thus, it is a tool that can be used to design the configuration of a green roof.

Keywords: green roof substrate, water retention curve, hydraulic conductivity, thermal conductivity, coupled water and heat flow, urban sustainability

2.2 Introduction

Green roofs have become widely adopted over the past 20 years as a technological response to a wide public concern towards sustainable development, controlling greenhouse gas emissions and increasing energy efficiency (Hashemi et al., 2015). They integrate vegetation into buildings helping to minimize some negative impacts of urbanizations (Raji et al., 2015). A properly designed green roof can decrease environmental pollution, noise levels, building energy consumption, and stormwater runoff (Vijayaraghavan, 2016), while they provide ecological services and increase urban biodiversity (Brown and Lundholm, 2015).

The overall performance of green roofs depends on the interaction between environmental conditions and the biophysical components of green roofs (Raji et al., 2015). Nevertheless, a myriad of choices for green roof construction are available, including alternatives for vegetation, substrates and membranes. A quantitative understanding of the processes that occur in each component of the green roof, and under site-specific climatic conditions is needed to realize one or more of the benefits mentioned above. This is particularly relevant in arid and semi-arid regions, where local materials may be different and climatic conditions greatly differ from humid regions, where most of the green roof research has been carried out to date (Peng and Jim, 2015).

The substrate and the vegetation layers are the most important components determining water and heat fluxes on green roofs (Buckland-Nicks et al., 2016). In this study, without detracting the important role that vegetation has on the hydraulic and thermal performance of a green roof, we focus on green roof substrates. The substrate is an engineered media that has an improved performance compared to natural soils (Brown and Lundholm, 2015). It provides critical resources for the vegetation: water, nutrients, and a support media (Campbell and Norman, 2013). The water retention capacity and the thermal behavior of a green roof strongly depend on the physical properties of the substrate, i.e., volumetric water content, bulk density, particle size distribution, mineralogical composition and texture of the soil (Assouline and Or, 2013; Charpentier, 2015). The heat flux across a green roof and the substrates moisture content

influence the heat gains and losses of buildings through the roof, which impacts the building energy consumption. Additionally, controlling the moisture content of the substrate is key for vegetation survival, especially in arid and semi-arid climates. Hence, to improve the overall performance of green roofs, it is important to characterize the physical, hydrodynamic and thermal properties of green roof substrates.

Many investigations have highlighted the importance of the substrate hydrodynamic properties, such as the water retention and hydraulic conductivity curves, on green roof behavior (Palla et al., 2009; Getter et al., 2011) but few have independently measured these properties (Charpentier, 2015; Brunetti et al., 2016), which are important to understand how water flows through the green roof substrate. Some studies have used hydrodynamic parameters from the literature to represent the water flow through the substrate (Hilten et al., 2008; Metselaar, 2012), while many have performed inverse modeling to estimate those parameters (Palla et al., 2009, 2011; Alfredo et al., 2010; Burszta-Adamiak and Mrowiec 2013; Li and Babcock, 2015). Remarkably, most of these studies have focused on the hydraulic behavior without taking into account the thermal performance of green roof substrates.

Although most investigations addressing thermal performance of green roofs consider the effects of moisture on the thermal properties of the substrate, they typically neglect the impact of water flow on the energy balance (Sailor, 2008; Sailor and Hagos, 2011). Sailor (2008) developed a model that simulates the heat fluxes within the substrate, including the energy exchange in the atmosphere-vegetation-substrate continuum. It was included in the simulation software EnergyPlus (U.S. DOE, 2016), a simulation tool widely used by practitioners to model energy consumption in buildings (Yaghoobian and Srebic, 2015; Silva et al., 2016). Though Sailor's model (2008) assumes that thermal properties depend on the substrate moisture, it considers that moisture within the green roof diffuses at a constant rate. Jaffal et al. (2012) developed another thermal model with similar assumptions than those of Sailor's model, while Sailor and Hagos (2011) and Zhao et al. (2014) included the effect of compaction on the thermal properties of the substrate. The assumption of constant moisture diffusion can seriously impair model estimations since the interplay between vegetation water

demands, time dependent atmospheric conditions, and the building internal temperature dynamics can introduce abrupt spatial and temporal changes in the moisture profile across the substrate. For this reason, the latest version of the EnergyPlus (U.S. DOE, 2016) software includes an advanced moisture diffusion calculation method. This moisture diffusion model is based on a solution of the Richards (1931) equation that uses the substrate hydrodynamic properties (Schaap and van Genuchten, 2006) to describe moisture transport within a green roof substrate. Nonetheless, this advanced model neglects the impact of water flow on the energy balance, only considering the effect of moisture on the substrate thermal properties.

Few studies have assessed the interactions between water and heat transport in green roof substrates (Charpentier, 2015; Sandoval et al., 2015). Charpentier (2015) measured the water retention properties of pozzolan and peat soils mixtures using a sand-suction table and a ceramic pressure plate (Klute, 1994), while the thermal properties of the substrate were estimated from the literature. Charpentier (2015) simulated water and heat fluxes using HYDRUS-2D (Šimůnek et al., 2016) and found that the thermal performance of green roofs was driven by the substrate water storage capacity. Sandoval et al. (2015) measured the hydraulic and thermal properties of different substrates and utilized HYDRUS-1D (Šimůnek et. al., 2006) to represent the water and thermal transport properties of a green roof. However, these studies did not include irrigation and/or drainage of the green roof when studying the thermal behavior of their system.

The general objective of this work is to investigate how the hydrodynamic and thermal properties of substrates influence the water and heat transport in green roof substrates considering all the water flow mechanisms found in green roofs. The specific objectives are: 1) to characterize a set of five organic (> 4% of organic matter) and mineral (< 4% of organic matter) green roof substrates in terms of their hydrodynamic and thermal properties: water retention curve, hydraulic conductivity curve, thermal conductivity, and specific heat capacity. The substrates were chosen due to their common use in green roofs (Pianella et al., 2016; Zhao et al., 2014) and their local availability; and 2) to evaluate the impacts of the previous properties on the water and

heat transport through green roof substrates using numerical simulations and including the effect of irrigation or drainage.

2.3 Materials and methods

In this section we describe the theory used to model the coupled water and heat transport, the green roof substrates selected for this study, and the methods used to determine the physical, hydrodynamic and thermal properties of the substrates.

2.3.1 Modeling coupled water and heat transport

The water flow in a green roof substrate was described using the classical Richards (1931) equation in a two-dimensional domain for a porous medium:

$$\frac{\partial \theta}{\partial t} = \frac{\partial}{\partial x}\left[K(\theta)\frac{\partial h}{\partial x}\right] + \frac{\partial}{\partial z}\left[K(\theta)\left(\frac{\partial h}{\partial z}\right)+1\right] \quad (2.1)$$

where θ is the volumetric water content; $K(\theta)$ is the hydraulic conductivity curve, i.e., the ease with which the water moves through the porous medium; h is the pressure head; x and z are the horizontal and vertical spatial coordinates, respectively; and t is the time. The water retention curve, $h(\theta)$, and the hydraulic conductivity, $K(\theta)$, are two key properties that control water flow in a variably saturated media (Campbell and Norman, 2013), and are needed to solve equation (2.1).

The water retention curve is a relationship between the pressure head, h, and the volumetric water content, θ. It is an important property of green roof substrates as it represents the capacity of the substrate to retain water. Substrates with larger water retention improves water use when irrigating green roofs and provides a moisture content more uniform for the vegetation. Thus, they contribute to vegetation development and survival, which is a critical aspect in post-plantation stages particularly

for arid and semi-arid climates (Vera et al., 2015). In this study, $h(\theta)$ was described using the van Genuchten (1980) model:

$$S_e = \frac{\theta - \theta_r}{\theta_s - \theta_r} = \frac{1}{\left(1 + |\alpha\, h(\theta)|^n\right)^m} \tag{2.2}$$

where S_e is the effective saturation; θ_r, and θ_s are the residual and saturated volumetric water contents, respectively; α is the inverse of the air-entry pressure; and n and m are empirical parameters.

The $K(\theta)$ was estimated using the van Genuchten-Mualem model with $m = 1–1/n$ (Mualem, 1976

$$K(\theta) = K_S S_e^l \left[1 - \left(1 - S_e^{1/m}\right)^m\right]^2 \tag{2.3}$$

where K_S is the saturated hydraulic conductivity, and l is the pore-connectivity parameter which is typically assumed to be 0.5 (Mualem, 1976).

The heat flow in a porous medium was described using the energy conservation principle (Saito et al., 2006):

$$C_p(\theta)\frac{\partial T}{\partial t} = \frac{\partial}{\partial x}\left[\lambda(\theta)\frac{\partial T}{\partial x}\right] + \frac{\partial}{\partial z}\left[\lambda(\theta)\frac{\partial T}{\partial z}\right] - C_w q_{lx}\frac{\partial T}{\partial x} - C_w q_{lz}\frac{\partial T}{\partial z} \tag{2.4}$$

where $C_p(\theta)$, and C_w are the volumetric heat capacities of the moist soil and water, respectively; T is the temperature; q_{lx} and q_{lz} are the liquid flux density in the horizontal and vertical directions, respectively; and $\lambda(\theta)$ is the soil apparent thermal conductivity, defined by (Jury and Horton, 2004):

$$\lambda(\theta) = \lambda_0(\theta) + \beta_t C_w |q_l| \tag{2.5}$$

where β_t is the thermal dispersivity; q_l is the magnitude of the liquid flux density; and $\lambda_0(\theta)$ is the thermal conductivity in absence of fluid flow. The $\lambda_0(\theta)$ was represented using the Chung and Horton (1987) model:

$$\lambda_0(\theta) = b_1 + b_2\theta + b_3\theta^{0.5} \tag{2.6}$$

in which b_1, b_2 and b_3 are empirical parameters.

2.3.2 Green roof substrates

The substrates investigated in this study are portrayed in Figure 2-1. The S1 substrate is similar to a sandy loam soil; the S2 substrate is comprised by perlite and peat; the S3 substrate has crushed bricks (clay); the S4 substrate is a mineral soil with tree leaves; and the S5 substrate is a mixture of topsoil and a mineral soil. These substrates were elected because of their common use in green roofs (S1-S3) and their local availability (S4 and S5). For instance, the S1 substrate has a mixture of sand and ~10% of compost that are known to increase the water holding capacity (Fassman-Beck et al., 2015). Substrates S1 and S3 have more than 80% of sand, which prevents the reduction of the saturated hydraulic conductivity with compaction (Fassman-Beck et al., 2015). The use of perlite (S2) in green roofs was analyzed by Zhao et al. (2014), while crushed bricks (S3) have been studied by Pianella et al. (2016) due to their high porosity and lightness.

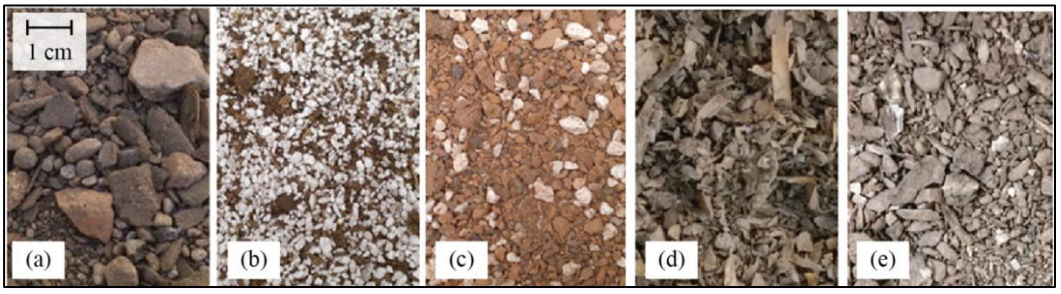

Figure 2-1:Substrates used in this study: (a) substrate S1; (b) substrate S2; (c) substrate S3; (d) substrate S4; and (e) substrate S5.

2.3.3 Physical, hydrodynamic and thermal properties of green roof substrates

a) Physical properties

The particle size distribution of the substrates was determined by sieving and hydrometer techniques (ASTM D422-63; Klute, 1994), and was used to calculate the texture, and the uniformity (C_u) and curvature (C_c) coefficients (Klute, 1994). The soil particle density (ρ_s) was estimated using the pycnometer technique (ASTM D 854-91; Klute, 1994) and the maximum soil density (ρ_{msx}) was measured using the Proctor compaction test (ASTM D1557-09).

b) Hydrodynamic properties

The water retention curve, $h(\theta)$, of each substrate was measured using the simplified evaporation method (Schindler, 1980). A substrate sample is subjected to evaporation under laboratory ambient conditions (average temperature of 22 ± 5 °C), while the water tension and the sample weight are recorded. The water retention curve between 0 and 1 bar is built using the relationship between the sample weight and the volumetric water content of the sample (Peters and Durner, 2006). We used the HYPROP® apparatus (UMS, Munich, Germany) to implement the evaporation method.

Substrate cores were inserted into 250 cm^3 stainless-steel cylinders (8 cm diameter and 5 cm height) and then slowly saturated from the sample bottom by placing them in a water reservoir with a 4.9-cm depth. Two tensiometers were inserted at depths of 1.25 and 3.75 cm, and the bottom of the substrate core was sealed. Each substrate core was installed on top of the weighing plate of a 0.01-g precision balance. The tensioVIEW software (UMS, Munich, Germany) was utilized to fit the water retention curve parameters of the van Genuchten model (1980) to the experimental data.

The van Genuchten-Mualem model (Mualem, 1976; van Genuchten, 1980) was used to estimate $K(\theta)$ (equation (2.3)). This model requires knowing K_s, the water retention curve parameters, and the pore-connectivity parameter. K_s was determined using the KSAT system (UMS, Munich, Germany), which is a constant- or variable-head permeameter that uses the same substrate cores as the HYPROP® apparatus. We used the permeameter with a variable head, and the Darcy equation was used to determine the K_s (Darcy, 1856).

c) Thermal properties

The substrates $\lambda(\theta)$ and $C_p(\theta)$ were obtained using a thermal properties analyzer (KD2 Pro, Decagon Devices, Pullman, WA) with a dual needle sensor (SH-1). The KD2 Pro system uses the dual-probe heat-pulse technique to determine the thermal properties (Bristow et al., 1994). In this technique, one of the needles has an internal heater that applies a heat pulse, while the other has a sensor that measures the thermal response of the media. This information is used to simultaneously estimate $\lambda(\theta)$ and $C_p(\theta)$ by solving the equation of radial heat conduction (Bristow et al., 1994). The thermal properties of the substrates were obtained for different volumetric water contents measured using the gravimetric method (Klute, 1994). All the substrate samples were carefully saturated from below, and once the samples were completely saturated, the thermal properties were measured in triplicate and the samples were weighed. These measures were repeated every 2-3 days while the substrate samples were dried naturally under the ambient conditions of a laboratory, until the samples were dry, i.e., after ~30 days. Then,

the samples were oven dried at ~80 °C (to avoid burning the organic matter) and weighed.

2.4 Results and discussion

2.4.1 Physical, hydrodynamic and thermal properties of substrates

a) Physical properties

Table 2-1 shows the physical parameters obtained for each substrate. In all the substrates, the majority of the particles correspond to sand (0.05-2 mm), followed by silt (0.002-0.05 mm) and then by clay (< 0.002 mm). According to the USDA, these substrates can be classified as sand, loam, sandy loam and loamy sand. The substrates particle densities (ρ_p) range between 2.13 and 2.51 g cm^{-3}, which are slightly less than natural minerals such as quartz (2.66 g cm^{-3}) and larger than organic matter (1.3 g cm^{-3}) (Balland and Arp, 2005). In addition, these values are similar to the ones found by Liu and Fassman-Beck (2016) in green roof substrates, with minimum values near to 2.21 g cm^{-3}. The observed maximum substrate bulk densities (ρ_{max}) range between 0.44 and 1.20 g cm^{-3}. These values are lower than those of natural soils, which typically range between 1.2-1.6 g cm^{-3} (Assouline, 2006a). However, green roof substrates bulk density values below 1 g cm^{-3} have been reported in the literature (Sailor and Hagos, 2011; Fassman-Beck et al., 2015; Liu and Fassman-Beck, 2016). The lower densities of the substrates compared to natural soils, are due to the addition of organic matter, tree leaves, wood and perlite, which are lightweight components commonly used in green roofs (Raimondo, 2015) that provide a large water storage volume (Li and Babcock, 2015). The organic compounds are also needed for the delivery of nutrients for plant growth. The lightness of the substrates is important to reduce loads in green roof infrastructure. International guidelines suggest the use of more than 80% of inorganic components to reduce infrastructure loads (FLL, 2002; DDC, 2007). In addition, a low-density substrate allows a thicker substrate layer where a wide variety of vegetation can

be planted (Vijayaraghavan, 2016). The large values of the uniformity coefficient C_u (between 43 and 240) indicate that the particle size distributions of all the substrates are highly heterogeneous. The C_u values are higher than the ones obtained by other green roof substrate (Liu and Fassman-Beck, 2016). According to the USDA, the S5 substrate can be classified as a well-graded soil (Klute, 1994), as opposed to the S1-S4 substrates that present curves that do not meet with that criteria.

Table 2-1: Texture according to the USDA soil classification system, soil particle density (ρ_s), maximum density (ρ_{max}), uniformity coefficient (C_u) and curvature coefficient (C_c) of the substrates used in this study.

Substrate	Soil type	Sand (%) 0.05-2 mm	Silt (%) 0.002-0.05 mm	Clay (%) <0.002 mm	ρ_p (g cm^{-3})	ρ_{max} (g cm^{-3})	C_u (-)	C_c (-)
S1	*Sand*	88.1	8.5	3.3	2.20	0.99	48	0.7
S2	*Sandy loam*	65.6	29.2	5.2	2.13	0.44	68	0.5
S3	*Loamy sand*	82.8	13.3	3.9	2.51	1.20	43	5.9
S4	*Loam*	50.7	34.4	14.9	2.44	1.13	240	0.6
S5	*Sandy loam*	53.4	37.6	9.0	2.32	0.98	89	1.2

b) Hydrodynamic properties

Figure 2-2 and Table 2-2 show the water retention curves of the five substrates and the fitted parameters of the van Genuchten model (1980). On one hand, the residual water content of substrates S4 and S3 is very small compared to substrates S1, S2, and S5. On the other hand, the saturated water content of all the substrates (S1-S5) is very large, ranging between 0.531 and 0.757 cm^3 cm^{-3}, and exceeded that of natural soils (0.374-0.500 cm^3 cm^{-3}) (Twarakavi et al., 2010). Note that the difference between the saturated and residual water contents represents the maximum water storage volume that a substrate can retain. Indeed, in a storm event the actual water storage volume in a substrate is the difference between the saturated water content and the water content prior to the storm. This water storage volume provides a retention time that temporarily stores a fraction of the potential runoff generated by the surface and it can significantly mitigate stormwater quality problems associated to stormwater runoff of small storms (Pitt and Clark, 2008). Substrate S4 has the largest water storage volume ($\theta_s - \theta_r$ = 0.62 cm^3 cm^{-3}), while substrate S1 has the smallest storage volume (0.45 cm^3 cm^{-3}). Other important parameter of the water retention curve is the air-entry pressure value $h_b = \alpha^{-1}$, which is the matric suction required for air to penetrate into the substrate when saturated. This property is important in green roof substrates because when drying conditions occur, substrates with larger values of h_b will retain water for longer time periods. Substrates S2 and S4 had air-entry pressures larger than 16 cm, while the others had air-entry pressure values lower than 9 cm.

Table 2-2. Hydrodynamic and thermal properties of the substrates.

Substrate	Hydrodynamic properties					Thermal properties			
	θ_r^* ($cm^3\,cm^{-3}$)	θ_s^* ($cm^3\,cm^{-3}$)	α^* (cm^{-1})	n^* (-)	K_s ($cm\,day^{-1}$)	b_1^{**} ($W\,m^{-1}\,K^{-1}$)	b_2^{**} ($W\,m^{-1}\,K^{-1}$)	b_3^{**} ($W\,m^{-1}\,K^{-1}$)	C_p ($MJ\,m^{-3}\,K^{-1}$)
S1	0.190	0.636	0.117	1.237	348	0.000	1.101	0.000	0.931
S2	0.179	0.757	0.059	1.561	1877	0.000	0.838	0.000	0.681
S3	0.001	0.531	0.328	1.233	2483	0.146	0.822	0.330	0.986
S4	0.001	0.623	0.041	1.649	172	0.125	0.000	0.922	0.911
S5	0.120	0.716	0.117	1.441	1380	0.000	1.166	0.030	0.807

* Parameters of the van Genuchten (1980) model for the water retention curve.

** Parameters of the Chung and Horton (1987) model for thermal conductivity.

According to the USDA classification, all the substrates studied in this work have h_b values within the typical range for sandy loams (30.2 cm), sands (15.98 cm), and loamy sands (20.58 cm) (Rawls et al., 1982).

In general, K_s values of the substrates ranging between 172 and 2483 cm day^{-1} (Table 2-2) are similar to those reported in the literature for other substrates used in green roofs (Li and Babcock, 2015). Substrates S1 and S4 have K_s values that are one order of magnitude smaller than the minimum values of K_s presented by Liu and Fassman-Beck (2016). The K_s value of S1 is on the same order than the USDA classification of natural soils (504 cm day^{-1}); however, S2 and S5 are two orders of magnitude larger than the corresponding values for sandy loams (62 cm day^{-1}). The K_s of S3 is also two orders larger than loamy sands (147 cm day^{-1}), while the K_s of S4 is one order of magnitude larger than loams (32 cm day^{-1}) (Rawls et al., 1982). Large values of K_s favor faster flows through the saturated substrate and thus the potential to mitigate storm-water runoff reduces under saturated conditions, unless a thicker substrate layer is used, as in the case of intensive green roofs (Vijayaraghavan, 2016).

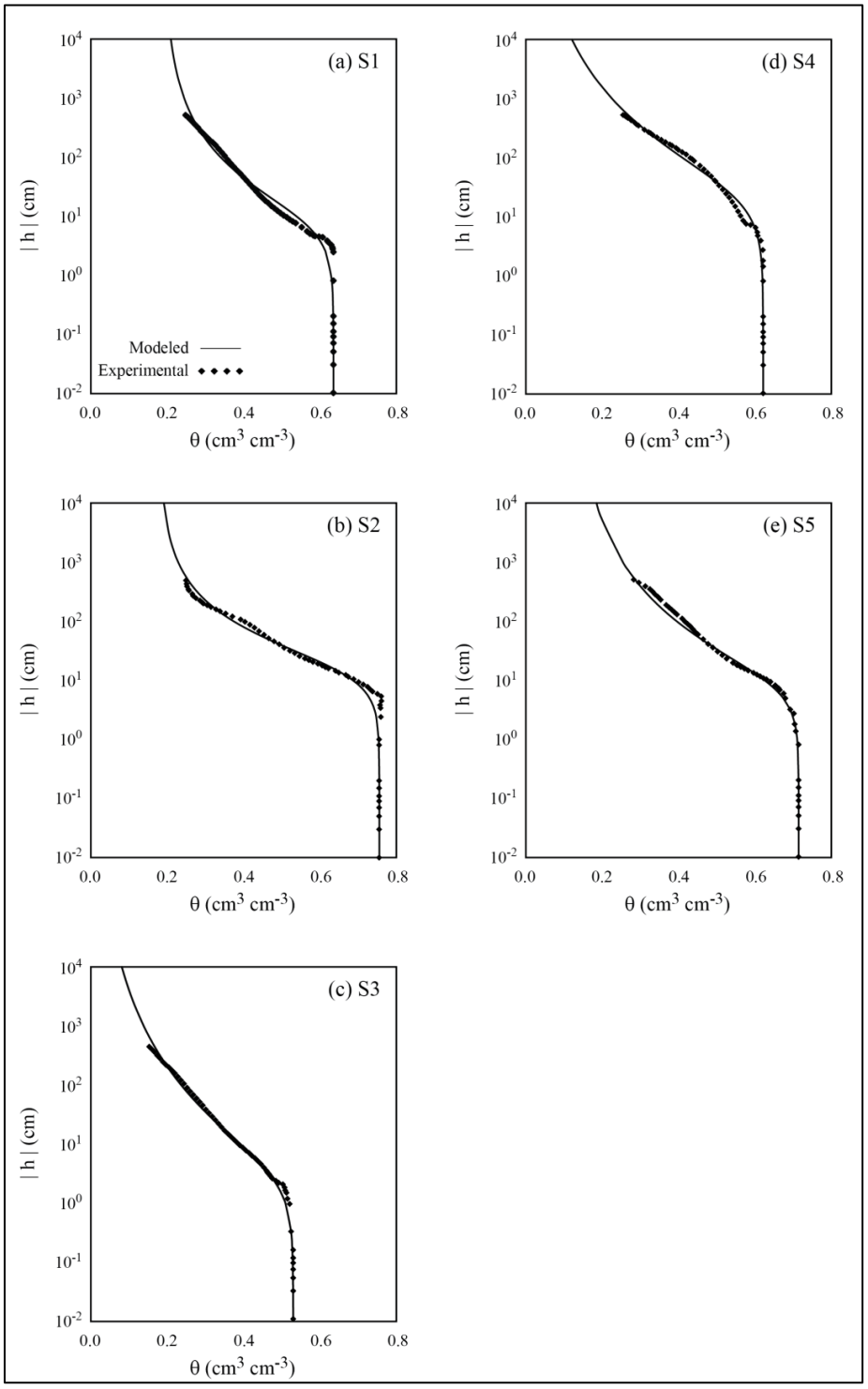

Figure 2-2: Water retention curves of substrates S1 (a), S2 (b), S3 (c), S4 (d), and S5 (e). Black diamonds are observations and solid lines are the modeled values.

c) Thermal properties

Figure 2-3 and Table 2-2 show the thermal conductivities of the substrates. The thermal conductivity values are similar to those of artificial substrates reported in the literature. Zhao et al. (2014) obtained thermal conductivity values between ~ 0.2 and ~1.4 W m^{-1} K^{-1} while Campbell and Norman (2013) reported values that ranged from ~0 to ~2.0 W m^{-1} K^{-1} for natural soils. The thermal conductivity of the substrates increases with moisture in different forms depending on the substrate. Such increase is linear with moisture, except for the S4 substrate. The linear increase in thermal conductivity occurs due to the organic nature of the substrates (Campbell and Norman, 2013). The thermal conductivity of substrates S3, S4 and S5 increases from ~0.1 to ~0.9 W m^{-1} K^{-1} for dry and saturated conditions, respectively; whereas the thermal conductivity of the S1 and S2 substrates ranges between ~0.2 and ~0.7 W m^{-1} K^{-1}. Thus, the thermal conductivity value is 5-8 times that of the dry thermal conductivity. These variations are similar to those obtained by Sailor and Hagos (2011), although the substrates investigated in this study show a larger water storage capacity. The S4 substrate has the largest water storage capacity and the largest fluctuation in its thermal conductivity. Consequently, its hydraulic and thermal behavior is expected to be more variable.

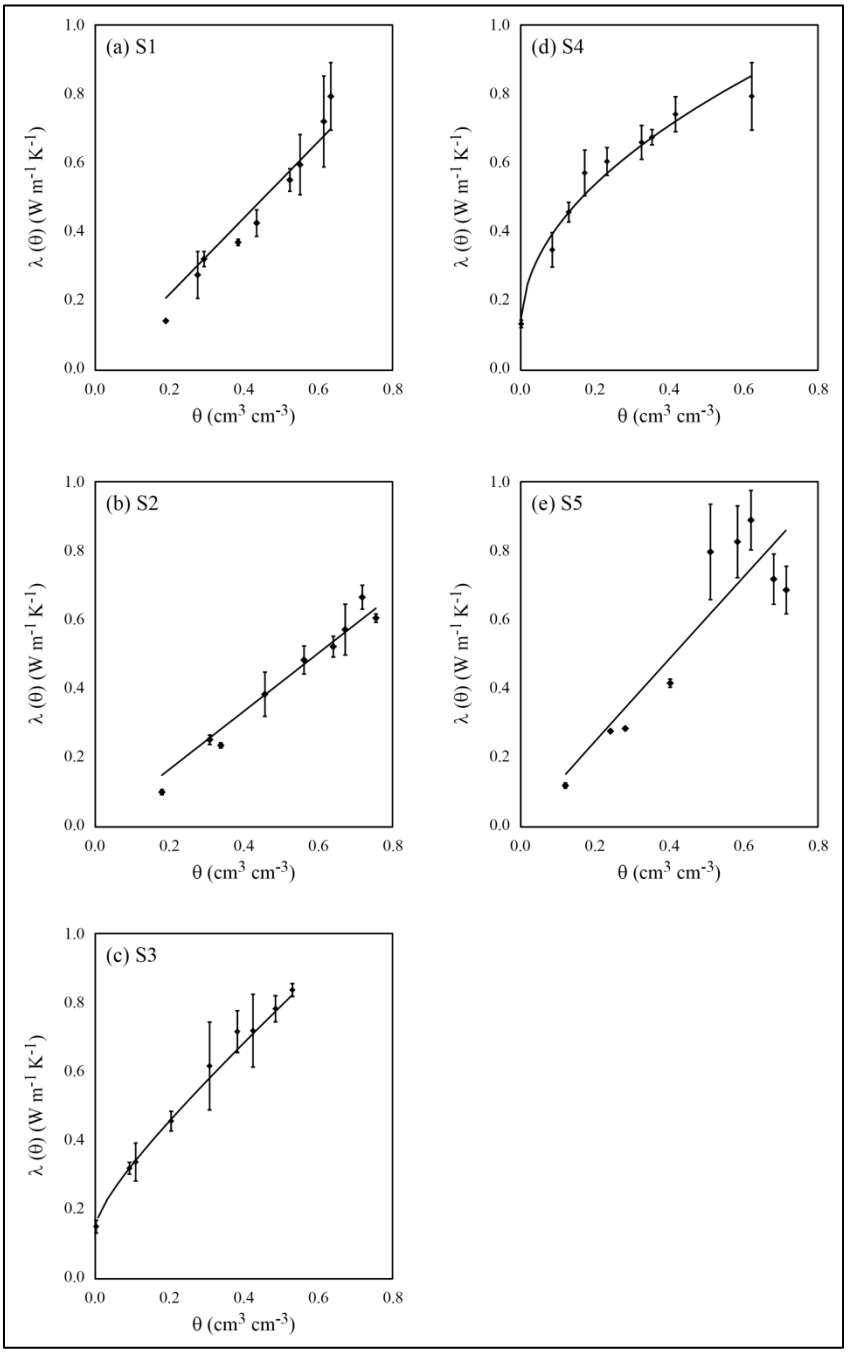

Figure 2-3.Thermal conductivity curves for substrates S1 (a), S2 (b), S3 (c), S4 (d), and S5 (e). Black diamonds are observations and solid lines are the modeled values. The error bars correspond to the standard deviation of three thermal conductivity measurements at each moisture level.

The volumetric heat capacity values (Table 2-2) indicate that the S2 substrate in a dry state is inappropriate to store heat, i.e., its vertical heat diffusion is large compared to the rest of substrates. Although in many porous media the volumetric heat capacity increases with moisture (Jury and Horton, 2004), the substrates S1, S2 and S5 showed constant values of thermal diffusivity as moisture increased (data not shown). This behavior occurs due to the linear behavior of the thermal conductivity of these substrates (Figure 2-3).

2.4.2 Simulation of water and heat transport through green roof substrates

To evaluate the impacts of the substrates physical, hydrodynamic and thermal properties on water and heat transport through green roof substrates, we performed numerical simulations of a hypothetical roof system comprised by a 15 cm height and 100 cm width substrate installed with a slope of 1% on top of a 20 cm thick concrete roof that is above a room. Figure 2-4 shows the conceptual model used to evaluate the impacts of the substrate properties on roof performance. This configuration replicates one of the available modules in the Laboratory of Vegetative Infrastructure of Buildings (LIVE for its acronym in Spanish) at Pontificia Universidad Católica de Chile. The LIVE is located in Santiago, Chile (33°26’S, 70°39’ W), in a region with a semi-arid climate (Reyes et al., 2016). We did not include the vegetation layer since we focused on isolating the differences between the hydraulic and thermal behaviors of substrates. Thus, we compared the hydraulic and thermal performance of the roof system when the different substrates (S1-S5) are used.

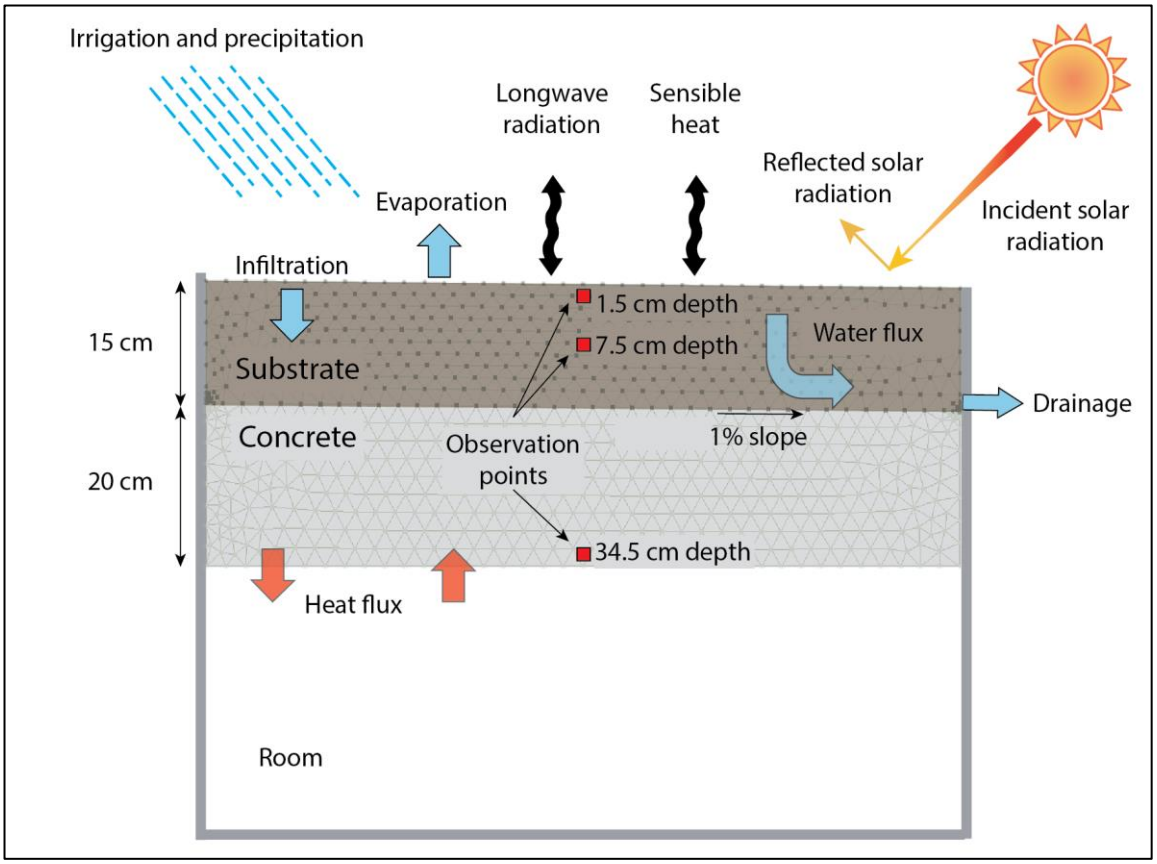

Figure 2-4.Green roof conceptual model used to run the numerical simulations. The numerical discretization used to solve the governing equations and the locations of observation points are also shown.

The coupled water and heat transport equations were solved using the HYDRUS-2D software (Šimůnek et al., 2016). The hydrodynamic and thermal properties of each substrate were defined according to the experimental results presented above, while the hydrodynamic and thermal properties of concrete were obtained from the literature (Lamond and Pielert, 2006; Schneider et al., 2012). A uniform and arbitrary initial substrate water content of 0.3 cm^{-3} cm^{-3} was selected for the water flow simulations. Precipitation, irrigation and evaporation were used as the flow boundary conditions at the top of the substrate. We considered the meteorological data measured at LIVE during one of the summer months (Figure 2-5) to define the previous boundary conditions. The irrigation program considered 10 mm day^{-1} distributed in three pulses

per day at 7 am, 2 pm, and 10 pm. The lateral boundary conditions were defined as impermeable walls, except in the zone where the drainage is located (Figure 2-5). This drainage was modeled using the seepage face boundary condition (Šimůnek et al., 2008), which assumes that there is no water flow as long as the pressure head is negative, and allows water to flow when the substrate becomes saturated. Under this last condition, atmospheric pressure is imposed at the boundary and the water flow is estimated using Darcy's Law (1856). The interface between the concrete layer and the room (Figure 2-4) was modeled using a no-flow boundary condition.

The cumulative water flow through the drain was used to compare the hydraulic performance of the different green roof substrates (S1-S5). The comparison was made by analyzing the breakthrough times (the first time when water exits from the drain), and the total volumes leaving the system.

The initial condition for the heat transport simulations was a uniform temperature equal to 23 °C. At the top of the domain, the surface energy balance was used as boundary condition for the heat transport equation (Šimůnek et al., 2008):

$$R_n = H + L_v E + G \tag{2.7}$$

where R_n is the net radiation, H is the sensible heat flux, E is the evaporation rate and G is the soil heat flux. It is important to note that equation (2.7) couples the water flow and the heat transport through the evaporation term, L_vE. Because HYDRUS-2D does not allow using the surface energy balance equation when coupling fluid flow and heat transport, we used the 1D version of the model, which does not have this limitation to solve equation (2.7) after assuming that evaporation is limited by the atmospheric conditions. Therefore, the resulting temperature at the top of the domain in the 1D simulations was used as the thermal boundary condition in the 2D simulations, and the evaporation rate –estimated with the soil resistance (Camillo and Gurney, 1986) and water vapor resistance (Campbell, 1985)– was used as the boundary condition for the water flow. Combining these boundary conditions ensures fulfilling the thermal surface energy balance. In each time-step, the validity of using the potential evaporation at the

substrate-atmosphere interface was assessed by comparing the equilibrium conditions between the water in the substrate pores and the atmospheric water vapor. This validation was based on the method proposed by on by Philip and de Vries (1957), in which the minimum pressure head in the substrate surface that ensures potential evaporation, h_A, is related to the air humidity, H_r, in the following way:

$$h_A = \frac{RT}{Mg}\ln\left(H_r\right) \tag{2.8}$$

where R is the universal gas constant, T is absolute temperature, M is the molecular weight of water, and g is the gravitational acceleration. The lateral heat transport boundary conditions were defined as adiabatic.

The thermal performance of the hypothetical roof system was assessed by assuming that the roof is over a single room that has adiabatic walls and floor, and determining the cumulative thermal energy (heating/cooling) required to maintain the room at a reference temperature T_{ref} = 23 °C. This thermal energy was calculated by performing an energy balance considering the convective heat flux that occurs between the ceiling and the room. Thus, the thermal convection occurring inside the room is the result of a difference between the room's bulk air temperature and the ceiling's temperature (Causone et al., 2009). The convective heat flux was determined using equation (2.9) (Causone et al., 2009):

$$\dot{Q} = h_c\left(T_c - T_{ref}\right) \tag{2.9}$$

where $\dot{Q}$ correspond to the convective heat flux through the ceiling (per m^2 of roof area), T_c is the temperature at the ceiling (i.e., at the bottom of the concrete layer), and h_c is a convective heat transfer, which depends on the thermal stratification that occurs inside the room. When $T_c < T_{ref}$, buoyancy forces induce natural convection inside the room resulting in large values of h_c; while when $T_c > T_{ref}$, low values of h_c are expected

due to a stable thermal stratification within the room. We used heat transfer coefficients of 3.75 and 0.5 W m^{-2} $°C^{-1}$ for $T_c < T_{ref}$ and $T_c > T_{ref}$, respectively (Causone et al., 2009).

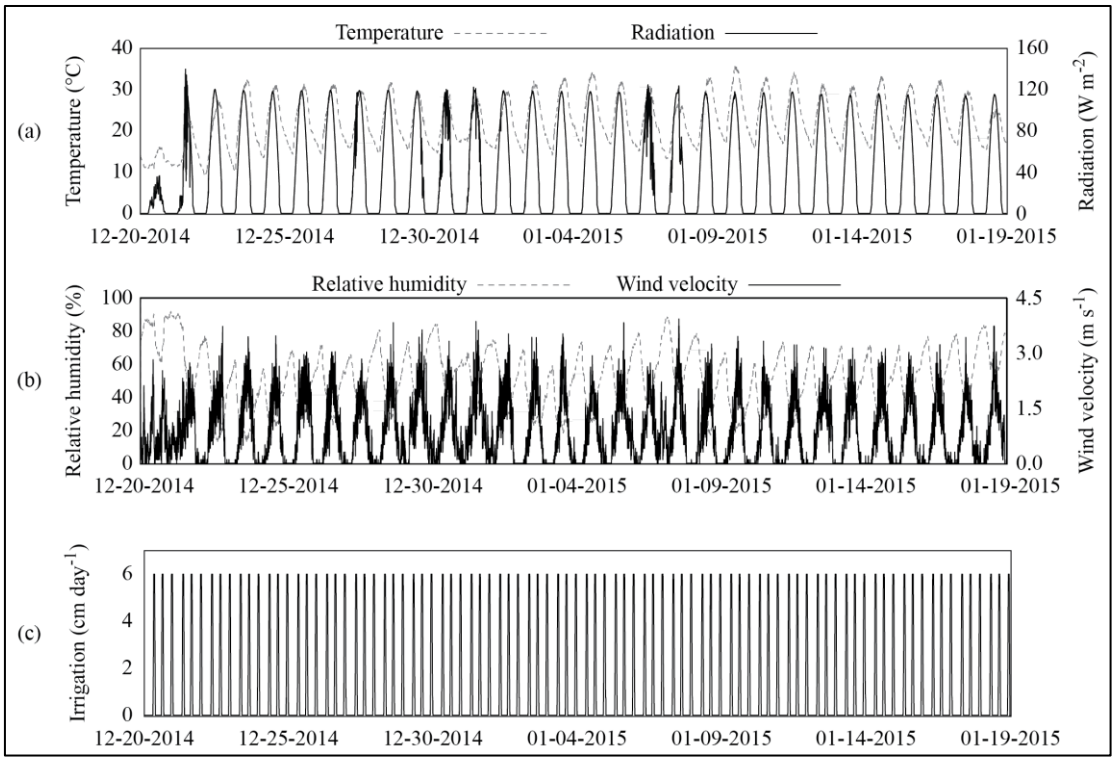

Figure 2-5: Meteorological and irrigation data used to drive the numerical simulations: (a) ambient temperature and solar radiation; (b) relative humidity and wind velocity; and (c) irrigation rate.

Figure 2-6 presents for each substrate the dynamics of the volumetric water content at the surface and at 10 cm below for the first five days of simulation. A daily cycle in all the substrates is observed, in which the water content increases after each irrigation and then decreases due to evaporation. Nevertheless, the same irrigation and meteorological conditions can produce different responses in each soil. For example, the substrates S1 and S4 present the larger moisture fluctuations at the substrate surface compared to the other substrates. In the second day of simulation, the surface moisture

in substrate S1 quickly decreases to 0.25 cm^3 cm^{-3}, most likely due to the high non-linearity of the water retention curve. At 10 cm depth, all the substrates present gradual moisture fluctuations with smaller amplitude than those occurring at the substrate surface. The moisture fluctuations during the first five days of simulation are mainly driven by irrigation and evaporation but not by drainage because the moisture content in all the substrates was less than saturation. The moisture of all substrates at 10 cm depth increases during the first five days of simulation. In addition, the amplitude of the moisture daily cycles is strongly related to the K_s. The S3 substrate presents the larger K_s and consequently, the larger daily variations of moisture at 10 cm depth. The moisture values during the first five days of simulation increase near to 0.4 cm^3 cm^{-3} for all the substrates except for S3. The substrate S3 showed the highest moisture content at 10 cm depth, most likely due to the closeness of the initial water content to the saturation water content of this substrate ($\theta_s - \theta_i$ = 0.23 cm^3 cm^{-3}), i.e., the S3 substrate saturates from the bottom before the rest of the substrates due to its smaller water retention capacity at low suctions (Figure 2-2c).

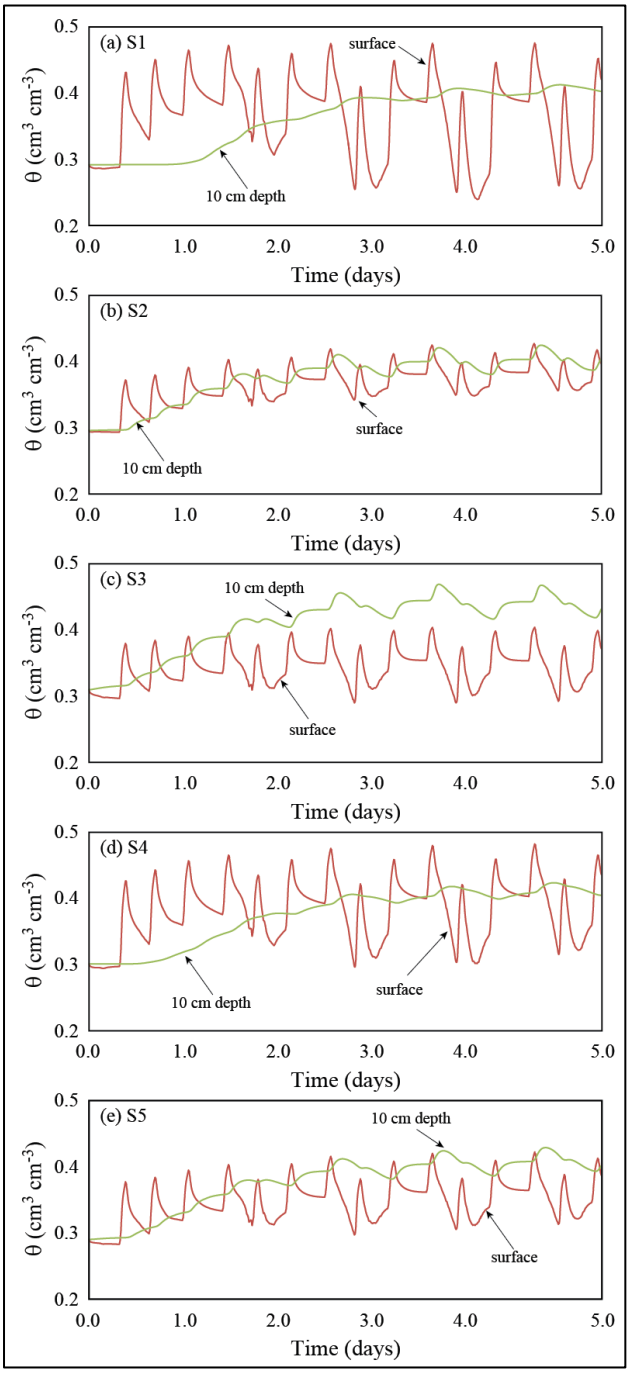

Figure 2-6. Evolution of the volumetric water content at different depths during the first five days of simulation for substrates S1 (a), S2 (b), S3 (c), S4 (d), and S5 (e). The red line depicts the water content at the substrate surface and the green line represents the water content at 10 cm depth.

Figure 2-7 shows the cumulative water flux that exits from the bottom of each substrate throughout the simulations. The water breakthrough at the drainage occurs at 3.6 days for the substrate S3, while substrates S1 and S4 take almost 23 days to release water through the drainage. The substrate S5 drains water after 27 days of simulation and S2 does not drain water during the simulation period. The substrates hydrodynamic properties explain this behavior. The main hydrodynamic property influencing the breakthrough time is the saturated water content: smaller saturated water content implies shorter breakthrough times and greater cumulative water fluxes. In addition, the magnitude of the cumulative water fluxes also depends on the properties of the water retention curve and the atmospheric conditions, which can dry the substrates in different ways depending on the retention characteristics of each substrate.

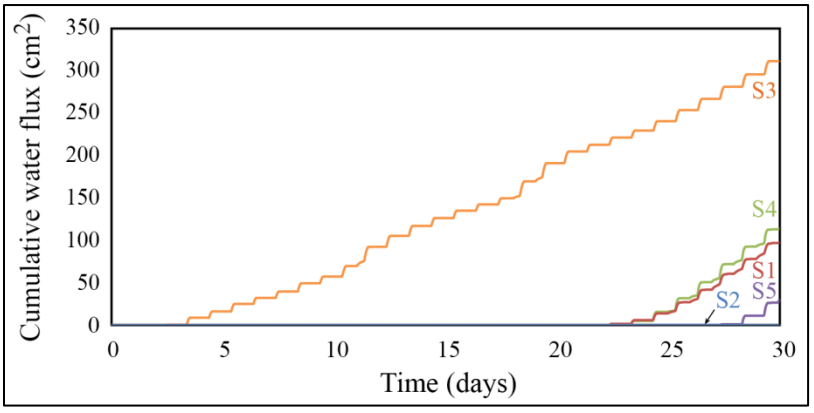

Figure 2-7. Cumulative water flux exiting through the drain of the roof system during the 30 days of simulation. Substrates are subject to the environmental conditions and a daily irrigation of 10 mm.

Figure 2-8a-e present the thermal evolution during the first five days of simulation at 1.5, 7.5 (substrate) and 34.5 cm (concrete) depth below the surface (Figure 2-4 shows the location of these observation points). The maximum values of the daily temperatures at the atmosphere-substrate interface reach ~35°C during the first five days of simulation and increase to more than 40°C during the entire simulation. Minimum daily temperatures at the substrate surface are similar to the air temperature (Figure 2-5),

except for the time between the first and the second day, when the temperatures at the substrate surface decline to ~5°C. The temperatures at the atmosphere-substrate interface of all the substrates are very similar. Figure 2-8f-j show the thermal envelope, i.e., the minimum and maximum temperatures at each depth within the roof system, using the different substrates for the 30 days of simulation. The minimum values are depicted in blue, the average values are represented in green, and the maximum values are shown in red. In general, the difference between the minimum and maximum temperatures at different depths reduces as depth increases. The magnitude of this difference is different for each substrate, showing the importance of the selection of the substrates. Note that this thermal amplitude should be reduced when adding the vegetation layer on top of the substrate (not analyzed here because it is out of the scope of this investigation). Our results show that the S1 and S2 substrates reduce more the thermal amplitude with depth than the rest of the substrates. The envelope of the S1 and S2 substrates is nearly symmetric, meaning that the thermal resistance of this substrate is similar for cooling or heating. At the surface of the S2 substrate a thermal amplitude of ΔT_s = 38.8°C is observed, while the range of thermal oscillations at the bottom of the concrete is ΔT_b = 9.5 °C. Note that the surface temperatures of S2 substrate oscillate the most of in response to the atmospheric conditions. However, the S2 substrate has a higher heat reduction capacity in the vertical direction trough the soil (77% amplitude reduction). In addition, the S2 substrate has the smallest variability at the bottom (ΔT_b = 9.2°C). On the other hand, the S3 substrate has the highest thermal variability at the bottom (ΔT_b = 11.9°C). The S4 substrate has the highest resistance to the atmospheric conditions (i.e., the smallest ΔT_s); however, it has the lower amplitude reduction with depth (68%).

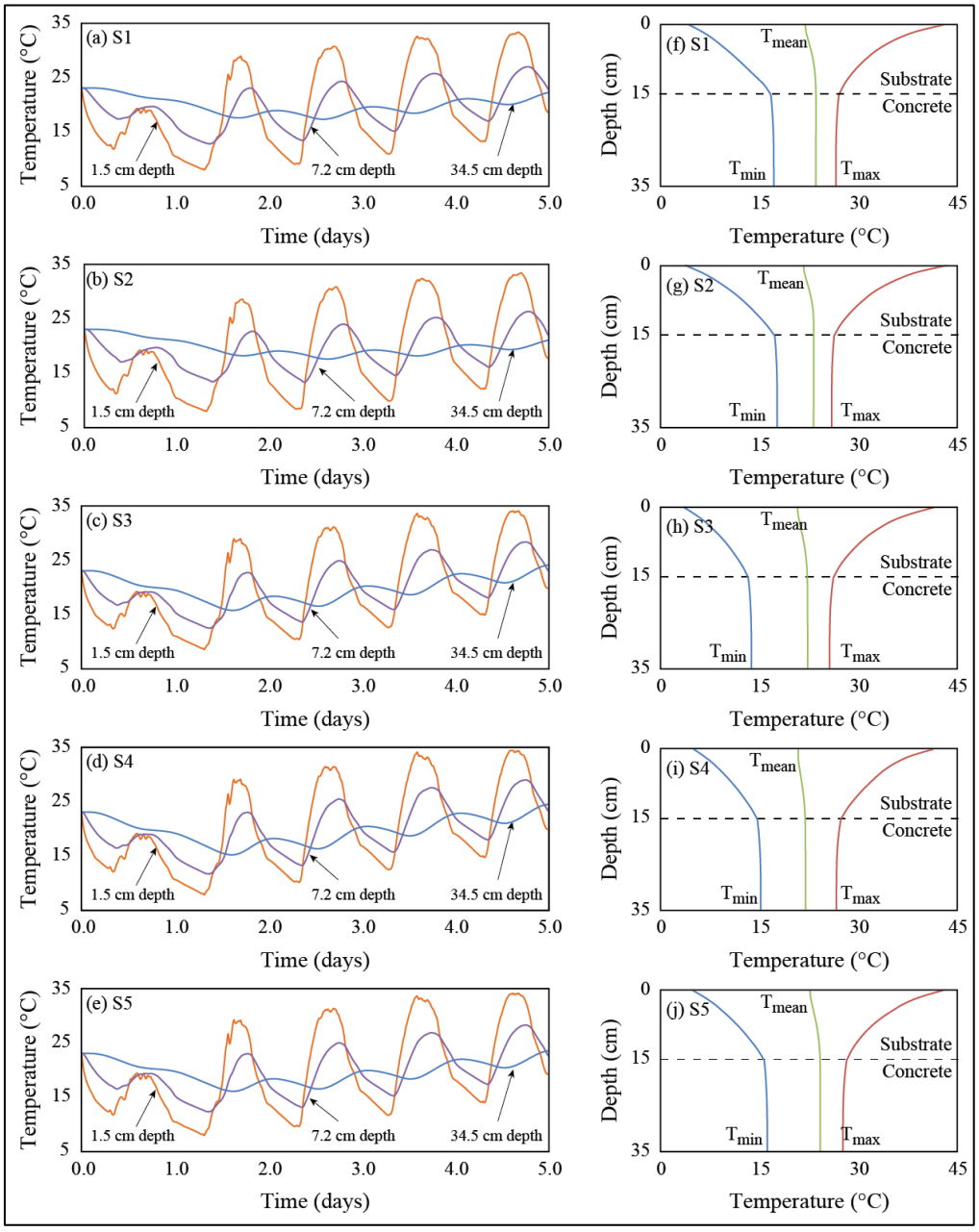

Figure 2-8. (a)-(e) Modeled temperatures at different depths in the five substrates (1.5 and 7.2 cm depth) and modeled temperature near the bottom of the concrete slab (34.5 cm depth), during the first five days of simulation. (f)-(j) Average temperature profile (T_{mean}, green line) and temperature envelope in the roof system during the entire simulation. Maximum temperatures (T_{max}) are depicted in red and minimum temperatures (T_{min}) are displayed in blue.

The hydrodynamic properties also impact the heat flux trough the substrate and concrete. Therefore, by analyzing the average values of humidity and thermal properties of the substrate composition, the processes related to heat and water flow can be better understood. The average values through the 30 days of simulation at 0.5 cm depth show that the substrates with more air and porosity behave very differently. The S4 substrate has an average moisture of 0.48 cm^3 cm^{-3}, with a thermal conductivity of 0.76 W m^{-1} K^{-1}, a volumetric heat capacity of 2.33 MJ $m^{-3}K^{-1}$ and a thermal diffusivity of 0.327 mm^2 s^{-1}. The percentage of the solid material in the substrate is 38% and the percentage of air is 14%. On the other hand, the S2 substrate has an average moisture of 0.44 cm^3 cm^{-3}, with a thermal conductivity of 0.44 W m^{-1} K^{-1}, a volumetric heat capacity of 2.02 MJ m^{-3} K^{-1}, and a thermal diffusivity of 0.217 mm^2 s^{-1}. The percentage of the solid matrix in this substrate is 25% and the air percentage is 31%. Hence, the S4 substrate has less air and more water and solid matrix than the S2 substrate, and thus conducts more heat. On the other hand, the S2 substrate has a lower diffusion than S4. The S2 substrate presents large differences in volumetric heat capacity depending on its moisture state; note that the dry soil value, 0.682 MJ m^{-3} K^{-1} increases to 2.016 MJ m^{-3} K^{-1} for a volumetric water content of 44.3% and a volumetric air content of 31.5%, highlighting the importance of the volumetric water and air contents on the thermal properties.

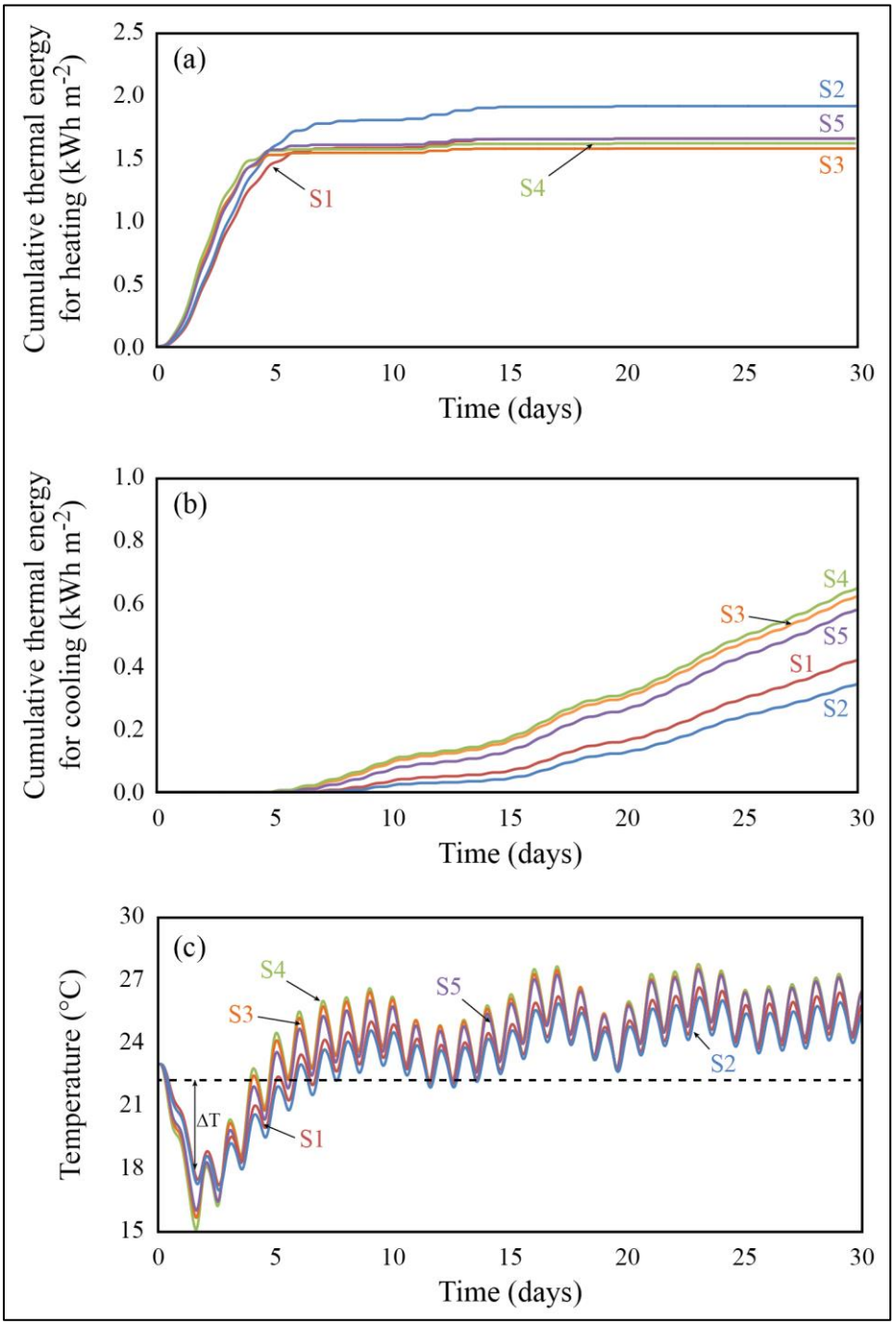

Figure 2-9. (a) Heating cumulative thermal energy required to maintain a reference room temperature of 23°C below the roof system. (b) Cooling cumulative thermal energy required to maintain a reference room temperature of 23°C below the roof system. (c) Modeled temperatures at 35 cm depth (bottom of the concrete) throughout the 30 days of simulation.

Figure 2-9a-b show the cumulative thermal energy (heating and cooling) consumed to maintain 23°C in the room below the roof system for the 30 days of simulation. As the convective heat flux depends on the ceiling temperatures, Figure 2-9c presents the thermal evolution at the bottom of the concrete layer of the roof system. During the first five days the ambient is cooler than the room and thus the room needs to be heated. Because the convective heat flux when $T_c < T_{ref}$ is larger than when $T_c > T_{ref}$ – due to natural convection driven by buoyancy (Causone et al., 2009), more thermal energy is needed to keep the room at the reference temperature (compared to the situation when $T_c > T_{ref}$, where a stable thermal stratification occurs in the room). After five days, the ambient temperature increases and thermal energy is now required to cool the room. The range of energy consumption for heating varied between 1.60 and 1.92 kWh m^{-2}, with the substrate S3 being the one that consumed less energy, and the substrates S1, S2 and S5 the ones that resulted in the highest energy consumption for heating. For cooling conditions, the energy consumption varied between 0.34 and 0.65 kWh m^{-2}, with the substrate S2 being the one that consumed less energy for cooling, and the substrates S3 and S4 had the highest cooling thermal energy consumption. In these simulations, the thermal energy required for cooling was less than that required for heating because the warmer temperatures simulated at the ceiling were ~3°C larger than T_{ref}, while the cooler temperatures were ~6°C cooler than T_{ref}.

The results of this investigation show that the S2 substrate is the one with the best capacity to store water. No water draining from S2 was simulated because of its large water storage capacity, due mainly to its large saturated water content. In terms of cumulative thermal energy, the substrate S2 decreases the cumulative thermal energy for cooling but increases the thermal energy for heating. The substrate S2 presents a low thermal conductivity and a large pore space. Hence, in dry conditions, the substrate S2 has an important fraction of air –and a low fraction of soil– within the pores, which reduces its thermal conductivity. In wet conditions the pores will be filled with water, which has a large volumetric heat capacity that reduces thermal diffusion within the roof. However, this last point could increase the energy consumption in winter

(Charpentier, 2015). These results suggest that the thermal behavior of a green roof substrate not only depends on its thermal properties but also on its hydrodynamic properties. Hence, the water/heat coupling must be accounted for when defining the substrate to be used in a green roof.

Although this study focuses on the hydraulic and thermal performance of green roof substrates, it is important to understand that some of the results presented here will change when a vegetation layer is added to a green roof. In this case, root water uptake will take place throughout the substrate profile according to the vertical root distribution, as opposed to what was modeled in our simulations where evaporation occurs at the substrate surface. Therefore, the moisture at the substrate surface will present less extreme values than those presented in this investigation (Figure 2-6). In addition, the vegetated green roof should dry less and slower than a non-vegetated roof, in a similar way than that described by Brunetti et al. (2016). Furthermore, since the evapotranspiration rate depends on the total plant resistance of each vegetation type (Campbell and Norman, 2013), it is likely that root water uptake will be smaller than the potential evapotranspiration rate that was used in this investigation. As a consequence, the suction within the substrate will be reduced and the average moisture level will increase. This increase in moisture content also increases the thermal conductivity of all the substrates (Figure 2-3). Nonetheless, it is expected that the thermal conductivity of the substrate S2 will remain smaller than that of the rest of the substrates. Also, when a vegetation layer is added to the roof, it is also expected to have lower temperatures at the substrate surface compared to those presented in this study (Figures 8a-e). These lower temperatures will be the result of the shadow made by leaves of the plants (e.g., see Getter et al., 2011).

2.5 Conclusions

In this study, the physical, hydrodynamic and thermal properties of five green roof substrates were determined experimentally and then used to understand their impact on the performance of a hypothetical roof system by means of numerical simulations.

All the substrates have large hydraulic conductivity values, which promotes water transmission through the green roof under saturated conditions. Nonetheless under unsaturated conditions, in addition to the substrate volume storage, the response of the roof to the atmospheric forcing is strongly dependent on the substrate water retention characteristics. The thermal conductivity of the substrates under investigation were on the same order of magnitude than those of other substrates reported in the literature, showing an important increase in the thermal conductivity as moisture increases. The heat transport trough the substrates strongly depends on the fraction of water, air and solid particles within the substrate, and the large water storage volume allows the attenuation of the diurnal thermal signal at the lowest boundary of the roof.

We found that the S2 substrate is the one with the best capacity to store water and to reduce storm-water runoff. In terms of cumulative thermal energy, the substrate S2 decreases the cumulative thermal energy for cooling but increases the thermal energy for heating. It presents a low thermal conductivity and a large pore space, which results in low thermal conductivity values for dry conditions. Nonetheless, under wet conditions its volumetric heat capacity reduces thermal diffusion within the substrate, which could increase energy consumption in winter.

Our results showed that the behavior of the hypothetical roof system strongly depends on its hydrodynamic and thermal properties, and highlight the importance of using dynamic modeling for design because of the complex interactions between the hydraulic and thermal processes that occur in green roof substrates. Future research should focus on studying the coupled partially saturated water flow and heat transport when the vegetation layer is added to the green roof.

3 A NEW METHOD TO DETERMINE HOW COMPACTION AFFECTS WATER AND HEAT TRANSPORT IN POROUS MEDIA – APPLICATION TO GREEN ROOF SUBSTRATES

3.1 Abstract

Although compaction affects the processes related to water and heat transport in porous media, there is a lack of investigations that deal with the effect of compaction on the coupled water and heat fluxes. Substrates are artificial porous media that are used for engineering and technological purposes. In this investigation, we studied the effect of compaction on the characterization of physical, hydrodynamic and thermal properties of five green roof substrates (S1-S5). The methodology of substrate compaction consists in a parametric analysis that uses the properties of a substrate with known bulk density, and then modifies the substrate properties to take into account how compaction affects water and heat fluxes. The substrate hydrodynamic properties in a compacted state show how the media's pore-size decreases, increasing the capillary forces and reducing the water storage volume. The impact of compaction on the thermal properties of the five green roof substrates agrees with the behavior reported in the literature for compaction in natural soils, even when the substrates are artificial media. The thermal conductivity in a compacted state shows a general increase compared to the uncompacted state. We performed coupled heat and water transport numerical simulations to assess the impact of the changes in the previous properties on the hydraulic and thermal performance of a hypothetical roof system. Results show that the S2 substrate presents the smallest vertical diffusion, which reduces the heat flux through the roof system. Only numerical simulations demonstrate the complexity of the behavior of each substrate and their response as compaction occurs when atmospheric conditions drive this system.

Keywords: green roof substrate, soil compaction, hydraulic properties, thermal conductivity, coupled water and heat flow, urban sustainability

3.2 Introduction

Soil compaction plays a key role in solute transport, nutrient availability, crop productivity and water movement (Alaoui et al., 2011). The compaction of soils has been typically investigated without considering its impact on the coupled water and heat transport in porous media (Zhou et al., 2012; Charpentier, 2015). There are many investigations that deal with the impact of compaction on water fluxes (Aravena et al., 2013; Augeard et al., 2008; Alaoui et al., 2011), as well as many studies that investigate how compaction affects heat fluxes in soils (Sailor and Hagos, 2011; Zhao et al., 2014). Nonetheless, there is a lack of studies that have investigated the effect of compaction on the coupled water and heat transport in substrates.

Substrates are engineered media that have improved performance compared to natural soils (Brown and Lundholm, 2015). They are typically used in many civil engineering applications. Their use in green roofs motivates this research because substrates provide water, nutrients and a support media for the vegetation (Campbell and Norman, 2013). Additionally, the water retention capacity and the thermal behavior of green roofs depend on the physical properties of the substrates (Sandoval et al., 2015).Therefore, to improve the overall performance of these systems is important to characterize the physical, hydrodynamic and thermal properties of green roof substrates and, in particular, the impact that substrate compaction has on water and heat transport in these systems.

Water transport in porous media usually is represented using the Richards (1931) equation:

$$\frac{\partial \theta}{\partial t} = \frac{\partial}{\partial x}\left[K(\theta)\frac{\partial h}{\partial x}\right] + \frac{\partial}{\partial z}\left[K(\theta)\left(\frac{\partial h}{\partial z}\right)+1\right] \tag{3.1}$$

where θ is the volumetric water content; $K(\theta)$ is the hydraulic conductivity curve; h is the pressure head; x and z are the horizontal and vertical spatial coordinates, respectively; and t is the time. The water retention curve, $h(\theta)$, and the hydraulic

conductivity curve , $K(\theta)$, are two important properties that control water flow in a variably saturated media (Campbell and Norman, 2013), and are needed to solve equation (3.1).

There are many expressions that can be used to represent the $h(\theta)$ (Brooks and Corey, 1964; van Genuchten, 1980; Assouline et al., 1998). The most used equation to represent the $h(\theta)$ is that proposed by van Genuchten (1980):

$$S_e = \frac{\theta - \theta_r}{\theta_s - \theta_r} = \frac{1}{\left(1 + |\alpha\, h(\theta)|^n\right)^m} \tag{3.2}$$

where S_e is the effective saturation; θ_r, and θ_s are the residual and saturated volumetric water contents, respectively; α is the inverse of the air-entry pressure; and n and m are empirical parameters. Assouline et al. (1998) also proposed a water retention model that has been used to investigate the impact of compaction on both $h(\theta)$ and $K(\theta)$; therefore, it is a relevant model for this investigation. The $h(\theta)$ model proposed by Assouline et al. (1998) is given in equation (3.3):

$$S_e(h) = \left\{1 - \exp\left[-\xi\left(|h|^{-1} - |h_L|^{-1}\right)^{\mu}\right]\right\} \qquad 0 \le h \le h_L \tag{3.3}$$

where ξ and μ are two fitting parameters, and h_L = 15 bar is the pressure head corresponding to a very low water content. It is also interesting to note that the parameters of the $h(\theta)$ models of Assouline et al. (1998) and van Genuchten (1980) can be related using the following expressions:

$$\mu = 0.51\,n^{1.1} \tag{3.4}$$

$$\xi = 1.21\,\alpha^{-1} \tag{3.5}$$

There are also many expression to represent the $K(\theta)$. The most used expression is the van Genuchten-Mualem model with $m = 1–1/n$ (Mualem, 1976):

$$K(\theta) = K_S S_e^l \left[1 - \left(1 - S_e^{1/m}\right)^m\right]^2 \tag{3.6}$$

where K_S is the saturated hydraulic conductivity, l is the pore-connectivity parameter which is typically assumed to be 0.5 (Mualem, 1976), and the S_e is determined using the van Genuchten (1980) model. Assouline and Tartakovsky (2001), on the other hand, describes the $K(\theta)$ using the following expression:

$$K(\theta) = K_S \sqrt{S_e}\left[\frac{\xi^{-1/\mu}\mu^{-1}\gamma\left(\mu^{-1}, \xi a_h\right) - h^{-1}\exp\left(-\xi a_h\right) + h_L^{-1}}{\xi^{-1/\mu}\mu^{-1}\Gamma\left(\mu^{-1}\right) + h_L^{-1}}\right]^2 \tag{3.7}$$

where γ and Γ are the incomplete and complete Gamma functions, respectively, and $a_h = \left[h^{-1} - h_L^{-1}\right]^{\mu}$.

The heat flow in a porous medium has been typically described using the energy equation (Saito et al., 2006):

$$C_p(\theta)\frac{\partial T}{\partial t} = \frac{\partial}{\partial x}\left[\lambda(\theta)\frac{\partial T}{\partial x}\right] + \frac{\partial}{\partial z}\left[\lambda(\theta)\frac{\partial T}{\partial z}\right] - C_w q_{lx}\frac{\partial T}{\partial x} - C_w q_{lz}\frac{\partial T}{\partial z} \tag{3.8}$$

where $C_p(\theta)$, and C_w are the volumetric heat capacities of the moist media and water, respectively; T is the temperature; q_{lx} and q_{lz} are the liquid flux density in the horizontal and vertical directions, respectively; and $\lambda(\theta)$ is the porous media apparent thermal conductivity, defined by (Jury and Horton, 2004):

$$\lambda(\theta) = \lambda_0(\theta) + \beta_t C_w |q_l| \tag{3.9}$$

where β_t is the thermal dispersivity; q_l is the magnitude of the liquid flux density; and $\lambda_0(\theta)$ is the thermal conductivity in absence of fluid flow. The volumetric heat capacity

of the moist soil, $C_p(\theta)$, is determined using the weighted average between the different phases that are present in the media, and can be described using the following equation (Jury and Horton, 2004)

$$C_p(\theta) = C_n\theta_n + C_o\theta_o + C_w\theta + C_a a_v \approx C_n\theta_n + C_o\theta_o + C_w\theta \quad (3.10)$$

where C is the volumetric heat capacity; a_v is the air content; the subscripts n, a, and w refer to the solid, air, and liquid phase, respectively; and the subscript o refers to organic matter. To represent the water and heat flux through porous media, as described in equations (3.1) and (3.8), both the hydrodynamic and thermal properties of the media must be known.

The objective of this study is to develop a methodology that can be used to represent the effect of compaction on the hydrodynamic and thermal properties of a porous medium. The new methodology combines the Richards (1931) and the energy equations to predict water and heat fluxes in a compacted medium. Through the use of numerical simulations populated with experimental data obtained from green roof substrates, the proposed methodology is used to predict water and heat fluxes in a hypothetical roof system and to determine the heat required to maintain a constant reference temperature in a room located below the roof.

3.3 Materials and methods

In this section we describe the theory used to incorporate the effect of compaction on the hydrodynamic and thermal properties of porous media, which can then be used to determine the impact of substrate compaction on water and heat transport. Then, we describe the substrates used to apply this methodology.

3.3.1 Impact of compaction on the hydrodynamic properties

To consider the effect of compaction on the water retention curve, the method proposed by Assouline (2006a) was employed. In this method, a homogeneous porous medium with an initial bulk density, ρ, is compacted to a density ρ_c. After the porous medium is compacted, the compacted saturated and residual water contents, θ_{sc} and θ_{rc}, respectively, are calculated has follows:

$$\theta_{sc} = \theta_s \left[\frac{\rho_s - \rho_c}{\rho_s - \rho} \right] \tag{3.11}$$

$$\theta_{rc} = \theta_r \left(\frac{\rho_c}{\rho} \right) \tag{3.12}$$

where ρ_s is the solid particle density of the substrate. When the porous media is compacted, Assouline (2006a) proposed to estimate the change in the remainder parameters of his water retention curve as follows:

$$\xi_c = \xi \left(\frac{\rho_c}{\rho} \right)^{3.72} \tag{3.13}$$

$$\mu_c = \mu \left(\frac{\rho_c}{\rho} \right)^{w} \tag{3.14}$$

$$w = 2.3 - 1.9 \left(\frac{\mathrm{SC}}{\mathrm{CC}} \right)^{0.55} \tag{3.15}$$

where the subscript *c* refers to the compacted state, and *w* represents the effect of the silt content (SC) and the clay content (CC) on the way that the porous medium is compacted. Equations (3.13) and (3.14) can be also written using the α and *n* parameters of the van Genuchten (1980) model:

$$\frac{\alpha}{\alpha_c} = \left(\frac{\rho_c}{\rho}\right)^{3.72} \tag{3.16}$$

$$\frac{n_c}{n} = \left(\frac{\rho_c}{\rho}\right)^{0.91w} \tag{3.17}$$

The effect of compaction on the saturated hydraulic conductivity was estimated using the approach presented by Assouline (2006b). He proposed obtaining the saturated hydraulic conductivity for a compacted bulk density using the following expression:

$$\frac{K_{Sc}}{K_S} = \frac{\left\{(\theta_{sc} - \theta_{rc})\left[\zeta_c^{-1/\mu_c}\mu_c^{-1}\Gamma(\mu_c^{-1}) + |h_L|^{-1}\right]\right\}^{\eta_c}}{\left\{(\theta_s - \theta_r)\left[\zeta^{-1/\mu}\mu^{-1}\Gamma(\mu^{-1}) + |h_L|^{-1}\right]\right\}^{\eta}} \tag{3.18}$$

with $\zeta = \xi^{\mu}$, and where η is a parameter that depends on the coefficient of variation of the water retention model of Assouline (2006b):

$$\eta = 3.04\exp\left(-\frac{\sigma}{r_G}\right) \tag{3.19}$$

where σ^2 and r_G are the second and first moments of equation (3.3):

$$r_G = \zeta^{1/\mu}\Gamma(1+1/\mu) + 1/|h_L| \tag{3.20}$$

$$\sigma = \left\{\zeta^{1/\mu}\left[\Gamma(1+2/\mu) - \Gamma^2(1+1/\mu)\right]\right\}^{1/2} \tag{3.21}$$

The calculation of K_{Sc}/K_s requires the utilization of equations (3.19)-(3.21) to find the parameters for the uncompacted and compacted state, and the values of μ and μ_c from equation (3.14). Through the use of equations (3.16) and (3.17), the parameters of

the Assouline (2006b) model in the compacted state can be related to those of the van Genuchten (1980) water retention curve.

3.3.2 Impact of compaction on the thermal properties

After knowing the thermal conductivity curve as a function of S_e in an uncompacted porous media, e.g., a relationship such as that presented in equation (2.9), it is of interest to characterize the impact of the compaction in the thermal conductivity curve. I propose to use different theoretical approaches combined with empirical information to include the effect of compaction on the thermal conductivity curve. The Johansen (1975) model can be used to represent the thermal conductivity in absence of fluid flow, λ_0. This relationship depends on S_e and on the bulk density (ρ) of the media (Balland and Arp, 2005):

$$\lambda_0(S_e) = \left(\lambda_{0s} - \lambda_{0d}\right)\lambda_e + \lambda_{0d} \tag{3.22}$$

where λ_{0s} and λ_{0d} are the thermal conductivities in the saturated and the dry states, respectively; and λ_e is the Kersten number, defined as (Johansen, 1975; Coté and Konrad, 2005):

$$\lambda_e = \frac{\kappa S_e}{1+(\kappa-1)S_e} \tag{3.23}$$

where κ is an empirical parameter that depends on the soil type and does not change with ρ (Barry-Macaulay et al,.2015).

The λ_{0s} is estimated using the following expression (Johansen, 1975):

$$\lambda_{0s} = \lambda_{sol}^{(1-\theta_s)}\lambda_w^{\theta_s} \tag{3.24}$$

where λ_w is the water thermal conductivity and λ_{sol} is the thermal conductivity of the solid particles. Equation (2.24) assumes that the porosity of the porous media is similar to its saturated volumetric water content.

The λ_{0d} is determined using the Balland and Arp model (2005), which is suitable for any type of soil:

$$\lambda_{0d} = \frac{(a\lambda_{sol} - \lambda_{air})\rho + \lambda_{air}\rho_s}{\rho_s - (1-a)\rho} \tag{3.25}$$

where a is an empirical parameter, ρ is the bulk density, ρ_s is the particle density of the porous media, and λ_{air} is the thermal conductivity of air.

The thermal conductivity curve in absence of fluid flow for the compacted porous media, $\lambda_c(\theta)$, needs some inputs from the hydrodynamic properties: first, to determine λ_{0s}, the θ_s is required, as shown in equation (3.24); and second, the lower and upper bounds of the thermal conductivity curve are related to the θ_r and θ_s that also change as compaction occurs. Also, note that the impact of compaction on the $\lambda_c(\theta)$ is represented through the bulk density that is used to determine λ_{0d}, but also through the change in the θ_s described in equation (3.11), which modifies the λ_{0s}.

The compaction methodology proposed in this investigation requires the use of empirical data to determine how the thermal conductivity changes as compaction occurs. First, the thermal conductivity curve must be known for a specific ρ, i.e., the values of $\lambda_0(S_e)$, λ_{0s} and λ_{0d} are known. Combining this information with equation (3.22) allows finding the Kersten number (λ_e) for different saturation degrees. Then, equation (3.23) is used to find the value of κ that represents the best the λ_e for each porous media. Recall that κ does not change with ρ (Barr-Macaulay et al,.2015). According to Coté and Konrad (2005) the value of κ depends on soil type; well-graded gravels and coarse sands have $\kappa \approx 4.6$, silts and clays have $\kappa \approx 1.9$ and peat has a $\kappa \approx 0.6$. In this study, we used the κ value as a fitting parameter to obtain a λ_e (S_e) for each substrate that agrees with the experimental information. Later, equations (3.24) and (3.25) are used to find the value of λ_{sol} that matches better the thermal conductivity curve of each porous medium, and to find the value of a that represents the behavior of all the porous media.

The change in the volumetric heat capacity of the porous media as compaction occurs can be readily considered using equation (3.10) by modifying the saturated water content as described in equation (3.11).

3.3.3 Substrates

To evaluate the proposed methodology that investigates the impact of compaction on the coupled water and heat flux, empirical information from five substrates was used. The substrates used in this study are depicted in Figure 2-1. These substrates were selected because of their common use in green roofs (S1-S3) and their local availability (S4 and S5). A detailed characterization of the physical, hydrodynamic and thermal properties of these substrates is presented in Chapter 2. Table 2-1 presents a summary of the physical properties of each substrate for their uncompacted state; and Table 2-2 shows the hydrodynamic and thermal properties of these substrates for an uncompacted state. For a comprehensive presentation of the methods used to determine the previous properties in the uncompacted state, the reader is referred to Chapter 2 of this thesis.

3.3.4 Influence of substrate compaction on the performance of a hypothetical roof system

To evaluate the impacts of substrate compaction on water and heat transport through green roof substrates, we carried out numerical simulations in the same hypothetical roof system investigated in Chapter 2. As the simulations reported in this study use the same domain and boundary conditions described before, here we only provide a brief description of the numerical model. Figure 2-4 presents the conceptual model utilized to investigate the effect of substrate compaction on roof performance. The system is comprised by a substrate on top of a concrete layer that is above a room. As we focused on substrate compaction, we did not include the vegetation layer on this system. Instead, we put our attention in analyzing the effect of compaction on the

performance of the roof system when the five substrates investigated in this study are employed.

The coupled water and heat transport (equations (3.1) and (3.8)) were solved using the HYDRUS-2D software (Šimůnek et al., 2016), and considering the uncompacted and compacted hydrodynamic and thermal properties for each simulation. The uncompacted hydrodynamic properties of the substrates were defined according to the experimental values reported in Chapter 2, while the compacted properties were determined according to the proposed model. The hydrodynamic and thermal properties of the concrete were defined using the information reported by Lamond and Pielert (2006) and by Schneider et al. (2012). In all the simulations, a uniform and arbitrary initial moisture content of ~0.3 cm^3 cm^{-3} was selected. The flow boundary conditions at the top of the domain were defined using the precipitation, irrigation, and evaporation measured at LIVE during one month. The irrigation schedule considered 10 mm day^{-1} allocated in three pulses per day at 7:00, 14:00, and 22:00 hrs. The information related to the previous boundary condition is presented in Figure **2-5** (see Chapter 2). The lateral boundary conditions were defined as impermeable boundaries, except where the drainage is located. The seepage boundary condition (Šimůnek et al., 2008) was used to represent the drain and the interface between the concrete layer (ceiling) and the room was represented with a no-flow boundary conditions. The cumulative water flow through the drain was used to compare the hydraulic performance of the different green roof substrates (S1-S5).

The initial condition for the heat transport simulations was a uniform temperature equal to 23 °C. At the top of the domain, the surface energy balance was utilized as boundary condition for the heat transport equation (Šimůnek et al., 2008). The lateral heat transport boundary conditions were defined as adiabatic. The thermal performance of the hypothetical roof system was evaluated by considering that the roof is above a single room with adiabatic walls and floor, and using the cumulative thermal energy (cooling/heating) required to keep the room at a reference temperature T_{ref} = 23 °C. This thermal energy balance was estimated considering the convective heat flux that occurs

between the ceiling and the room, as described by Causone et al. (2009). The reader is referred to Chapter 2 of this thesis for a detailed description of the simulations.

3.4 Results and discussion

3.4.1 Impact of compaction on the substrates hydrodynamic properties

Figure 3-1 shows the water retention curves of the five substrates using the van Genuchten (1980) model for different bulk densities, and Table 2-2 presents the parameters of the water retention models (van Genuchten, 1980; Assouline, 1998) for the uncompacted and compacted states of the substrates. The alterations in the water retention curve when the substrates are compacted are clearly seen in Figure 3-1 –the pores decrease their size, diminishing the θ_s and increasing the air-entry pressure ($h_b = \alpha^{-1}$) due to an increase in the capillary forces (Assouline 2006a). These changes in the porous media water retention capacity are consistent with the observations published in the scientific literature. For instance, in the S2 compacted water retention curve, the h_b increases from 17 to 526 cm, while the h_b of the S1 substrate increases from 9 to 53 cm. The increases in the h_b values are in the same order of magnitude than those reported by Assouline (2006a). However, the impact of compaction on the θ_r is not the same for all the substrates. S1, S2 and S5 show an increase between 0.05 and 0.07 cm^3cm^{-3} in θ_r as compaction occurs while S3 and S4 show an insignificant change. The reason of this change is that the original density values of θ_r of S3 and S4 are near to zero and the equation 2.12 uses the original density to determine the compacted values of θ_r. In addition, the changes in n and small changes in θ_r drive unexpected retention curves as we can see in Figure 3-1c: the compacted water retention curve of S3 (ρ = 1 g cm^{-3}) intercepts the uncompacted curve (ρ = 1.2 g cm^{-3}) at ~0.15 cm^3cm^{-3}, meaning that below this value the water retention decreases. However, as the pore size decreases, an increase in the capillary forces is expected and thus one would expect an increase in general water retention (Alaoui et al., 2011). This phenomenon most likely occurs because the properties of these artificial substrates are very different than those of natural soils,

which are the media used to develop the algorithms that predict the effect of compaction on the hydrodynamic properties (Assouline, 2006a). Therefore, for substrates S3 and S4 the proposed model may not be the best representation of how compaction influences the hydrodynamic properties. From the results obtained for substrates S1-S5 (Figure 3-1), we conclude that the proposed method yields results that are physically possible for volumetric water contents that are greater than 0.2 cm^3cm^{-3}.

Table 3-1. Hydrodynamic properties of the substrates used in this study. The first row of each substrate refers to the uncompacted values and the second row corresponds to the compacted values obtained with the parametric analysis.

Substrate	ρ ($g\ cm^{-3}$)	θ_r^* (-)	θ_s^* (-)	α^* (cm^{-1})	n^* (-)	K_s ($cm\ d^{-1}$)	ξ^{**} *(bar)*	μ^{**} *(-)*	w^{**} *(-)*	η^{***} *(-)*	ε^{***} *(-)*	ς^{***} *(-)*
S1	0.85	0.1900	0.64	0.1170	1.44	348	0.032	0.762		1.025	1.329	0.072
	0.99	0.2215	0.57	0.0190	1.90	239	0.056	1.035	1.996	1.382	0.962	0.051
S2	0.23	0.1790	0.76	0.0590	1.65	3690	0.086	1.445		1.120	1.132	0.094
	0.40	0.3110	0.69	0.0019	4.18	410	0.252	2.461	1.850	1.781	0.666	0.067
S3	1.00	0.0010	0.52	0.1600	1.33	1850	0.034	0.701		0.928	1.458	0.094
	1.20	0.0013	0.44	0.0175	1.85	1540	0.067	1.000	1.949	1.344	0.994	0.067
S4	0.85	0.0010	0.61	0.0270	1.35	172	0.114	0.709		0.946	1.432	0.210
	1.95	0.0014	0.57	0.0089	1.65	115	0.172	0.887	2.011	1.654	1.118	0.206
S5	0.51	0.1284	0.70	0.0510	1.75	1380	0.029	0.946		1.277	1.056	0.035
	0.70	0.1780	0.63	0.0041	3.07	442	0.098	1.749	1.882	1.912	0.579	0.017

* Parameters of the van Genuchten (1980) model for the water retention curve.
** Parameters of the Assouline (1998) model for the water retention curve.
*** Parameters of the Assouline (2006b) model for hydraulic saturated conductivity.

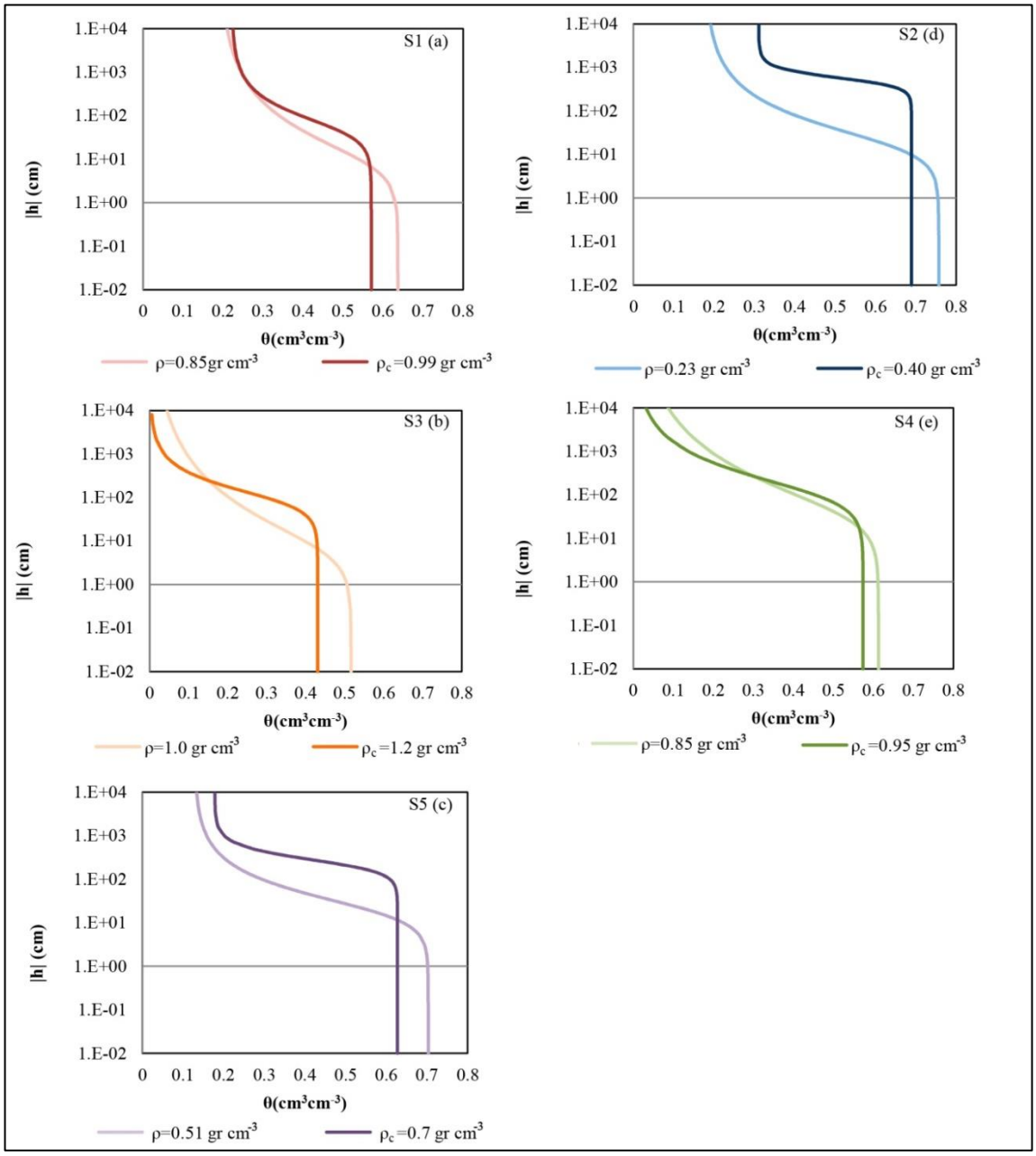

Figure 3-1:Water retention curves for the uncompacted (ρ) and compacted (ρ_c) substrates: (a) substrate S1; (b) substrate S2; (c) substrate S3; (d) substrate S4; (e) substrate S5.

3.4.2 Impact of compaction on the substrates thermal properties

To find how the thermal conductivity changes as compaction occurs, the first step in our methodology is to determine the λ_e, λ_{sol}, and κ for each substrate, and the a parameter for the set of substrates. Figure 3-2 presents the λ_e as a function of the S_e for each of the substrates investigated, estimated by fitting equation (3.23) to the experimental thermal conductivity data to find the κ parameter for each substrate; and by fixing the a parameter to 0.1614, which yields a good representation of the experimental values of λ_{0d} (equation (3.25)) for all the substrates. In this process, λ_{sol} was also fitted to represent correctly the thermal conductivity of each substrate and, in particular, the experimental values of λ_{0s} and λ_{0d}. Table 3-2 presents the values of κ and λ_{sol} obtained from this fitting process. In general, the values of κ are within the range of values reported for natural soils, and are typically in the range reported for silt, clay and peat (Coté and Konrad, 2005). The difference between the κ values obtained for the substrates used in this study and those reported for natural soils are most likely explained by the artificial nature of the substrates. The λ_{sol} values depend on the fraction of gravel, sand, silt, clay and percentage of quartz of each substrate. As a reference, soils with high organic matter have λ_{sol} ~0.25 W m^{-1} K^{-1}, while silty loam soils have λ_{sol} ~2.05 W m^{-1} K^{-1}, and crushed quartz has λ_{sol} ~7.2 W m^{-1} K^{-1} (Barry-Macaulay et al., 2015). The λ_{sol} presented in Table 3-2 ranges between 1.103 and 2.124 W m^{-1} K^{-1}. The lower values obtained for the λ_{sol} of each substrate, compared to natural soils, can be justified by the presence of organic matter and inorganic materials. The λ_{sol} values were fitted so the simulated λ_{0s} and λ_{0d} were similar to the experimental measures. This agreement between the simulated and experimental values was achieved in all the substrates except for substrate S2, where the fitted λ_{0d} (0.047 W m^{-1} K^{-1}) was lower than the measured λ_{0d} (0.101 W m^{-1} K^{-1}). However, the fitted and measured λ_{0s} of this substrate agreed with a difference of ~1%.

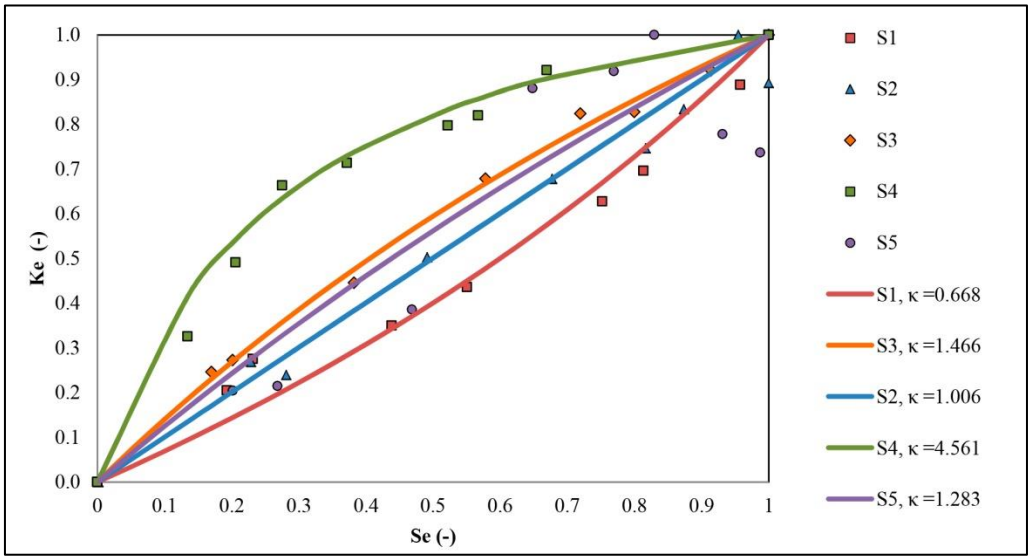

Figure 3-2: Kersten number (λ_e), which represents the normalized thermal conductivity curves of the five substrates investigated in this study. The λ_e values were obtained using the empirical data reported in Chapter 2. The κ values correspond to those of the Coté and Konrad (2005) model.

Table 3-2. Thermal properties of the substrates studied in this investigation. The first row of each substrate refers to the uncompacted state, while the second row corresponds to the compacted values obtained with the parametric analysis.

Substrate	ρ (g cm^{-3})	b_1^* (Wm^{-1}K^{-1})	b_2^* (Wm^{-1}K^{-1})	b_3^* (Wm^{-1}K^{-1})	κ** (-)	λ_{sol}*** (Wm^{-1}K^{-1})
S1	0.85	0.513	3.854	-2.769		
	0.99	1.026	5.780	-4.514	0.668	1.338
S2	0.23	-0.152	1.048	0.022		
	0.4	-0.690	2.212	0.115	1.006	1.103
S3	1.00	0.146	0.822	0.33		
	1.2	0.145	1.001	0.481	1.466	1.286
S4	0.85	0.125	0.000	0.929		
	0.95	0.154	0.000	0.987	4.561	1.382
S5	0.51	-0.286	0.552	0.889		
	0.7	0.199	0.000	0.954	1.283	2.125

* Parameters of Chung and Horton (1987) model for thermal conductivity: $\lambda_0(\theta) = b_1 + b_2\theta + b_3\theta^{0.5}$.

** κ parameter of equation (2.23)

*** λ_{sol} (Johannsen, 1985)

Figure 3-3 presents the thermal conductivity of the five substrates for both the uncompacted and the compacted state, and Table 3-2 shows the parameters of the Chung and Horton model (1987) –which was used to describe the thermal conductivity of the different porous media ($\lambda(\theta)$)–. In general, for a specific moisture level, as compaction occurs the thermal conductivity of the substrates increase. This behavior is consistent with the findings of other researchers (Sailor and Hagos, 2011; Zhao et al., 2014) and occurs because as the substrate is compacted, there is more physical contact between the solid particles, which increase thermal conduction (Jury and Horton, 2004; Aravena et al., 2014; Zhao et al., 2014). Also, the magnitude of the thermal conductivity is similar to that presented in the literature (Campbell and Norman, 2013; Zhao et al., 2014). Figure 3-3 also shows that substrates S2, S3 and S5 presents a linear increase of thermal conductivity with moisture, contrary to the non-linear behavior observed in substrates S1 and S4. In general, the impact of compaction on the thermal conductivity curve is more relevant in the saturated zone of the curve, i.e., when S_e approaches 1. For example, in substrate S2 the λ_{0s} increases in 0.17 W m^{-1} K^{-1} (~30% increase). In the dry zone of the curve, i.e., when S_e approaches 0, the substrates λ_{0d} present slight increases, with the exception of substrate S1, which shows an increment of 0.15 W m^{-1} K^{-1}. Similar effects are reported in other investigations, where the the thermal conductivity curves of different soils showed increases of 0.15 and of 0.4 W m^{-1} K^{-1} for λ_{0d} and λ_{0s} when the soil was compacted (Sailor and Hagos, 2011). However, previous investigations did not take into account the hydrodynamic effects of compaction on the conductivity curves. The addition of the hydrodynamic properties on the compaction method can be clearly seen in substrates S1 and S2 (Figure 3-3a,b). The highest change between the uncompacted and compacted thermal conductivity curves occurs in substrates S1 and S2. In S1, the increase in thermal conductivity is similar in all the range of the curve; contrary to what is observed for substrate S2, where the increment near the saturated part is too large while the increment near the dry part of the curve is too small. The small increment of the dry thermal conductivity in substrate S2 is due to its very low bulk

density (equation 3.25). In addition, the large change of density causes a large increment in θ_r (0.23 to 0.40 cm^3 cm^{-3}) (equation 3.12). As a result, the compacted and uncompacted curves intersect.

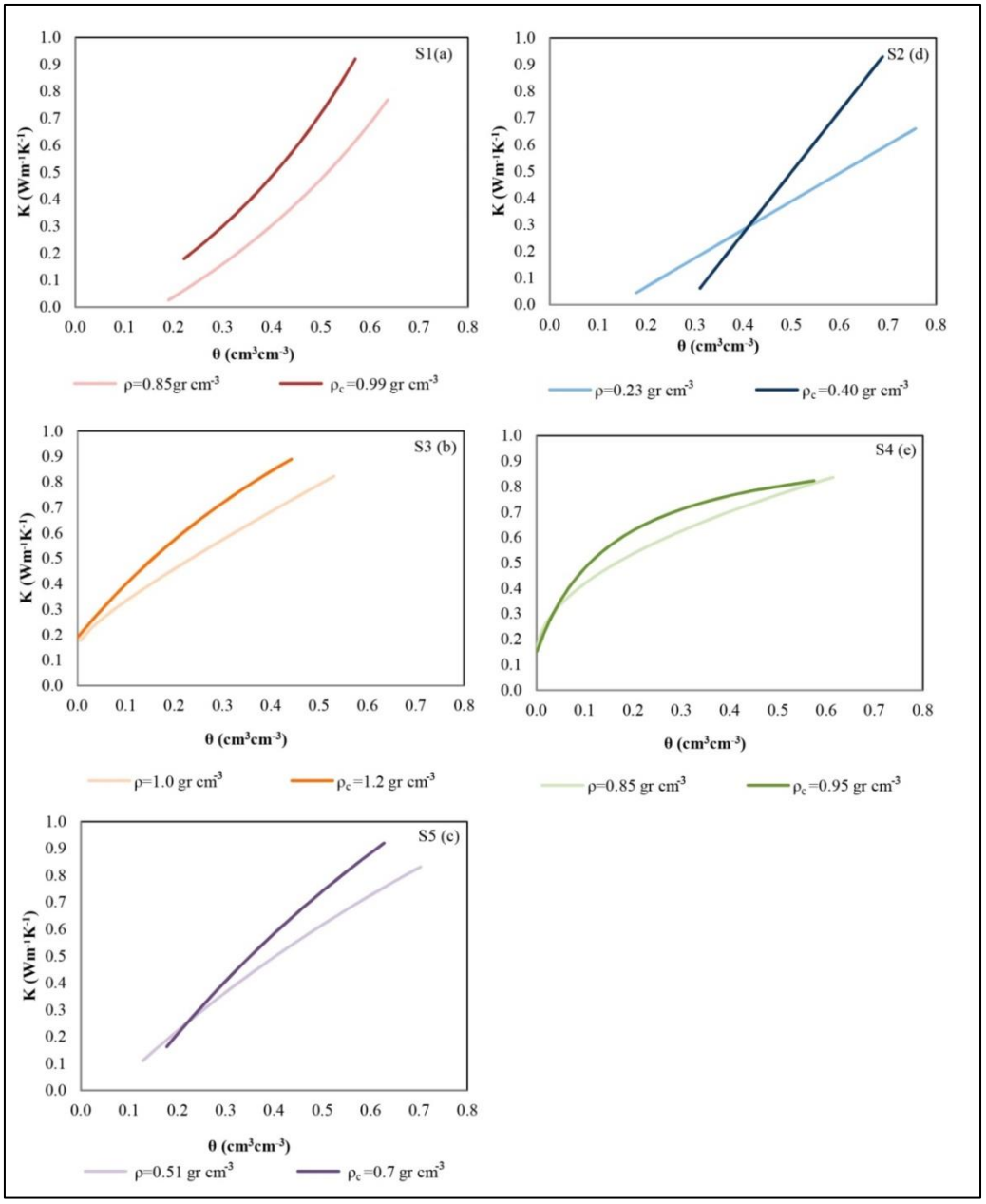

Figure 3-3: Termal conductivity curves for the uncompacted (ρ) and compacted (ρ_c) substrates: (a) substrate S1; (b) substrate S2; (c) substrate S3; (d) substrate S4; (e) substrate S5.

3.4.3 Influence of substrate compaction on the performance of a hypothetical roof system

Figure 3-4 shows the temporal evolution of the volumetric water content during the first five days of simulation at the atmosphere-substrate interface. Light colors correspond to the uncompacted substrate while dark colors are related to the compacted substrate. The water content evolution shows a daily cycle in all the substrates where the water content increases after the roof is irrigated, and then decreases due to evaporation. The effect of compaction on the moisture level is clear: in general, after the substrates were compacted, the fluctuations in the volumetric water content are smaller. The reduction in the moisture fluctuations is clear for substrates S1 and S4. On the other hand, for substrates S2, S3 and S5 the mean water content increases most likely due to the reduction of water storage volume. Figure 3-4 demonstrates that there is a change in the hydrodynamic response of each substrate to the same meteorological conditions as compaction occurs.

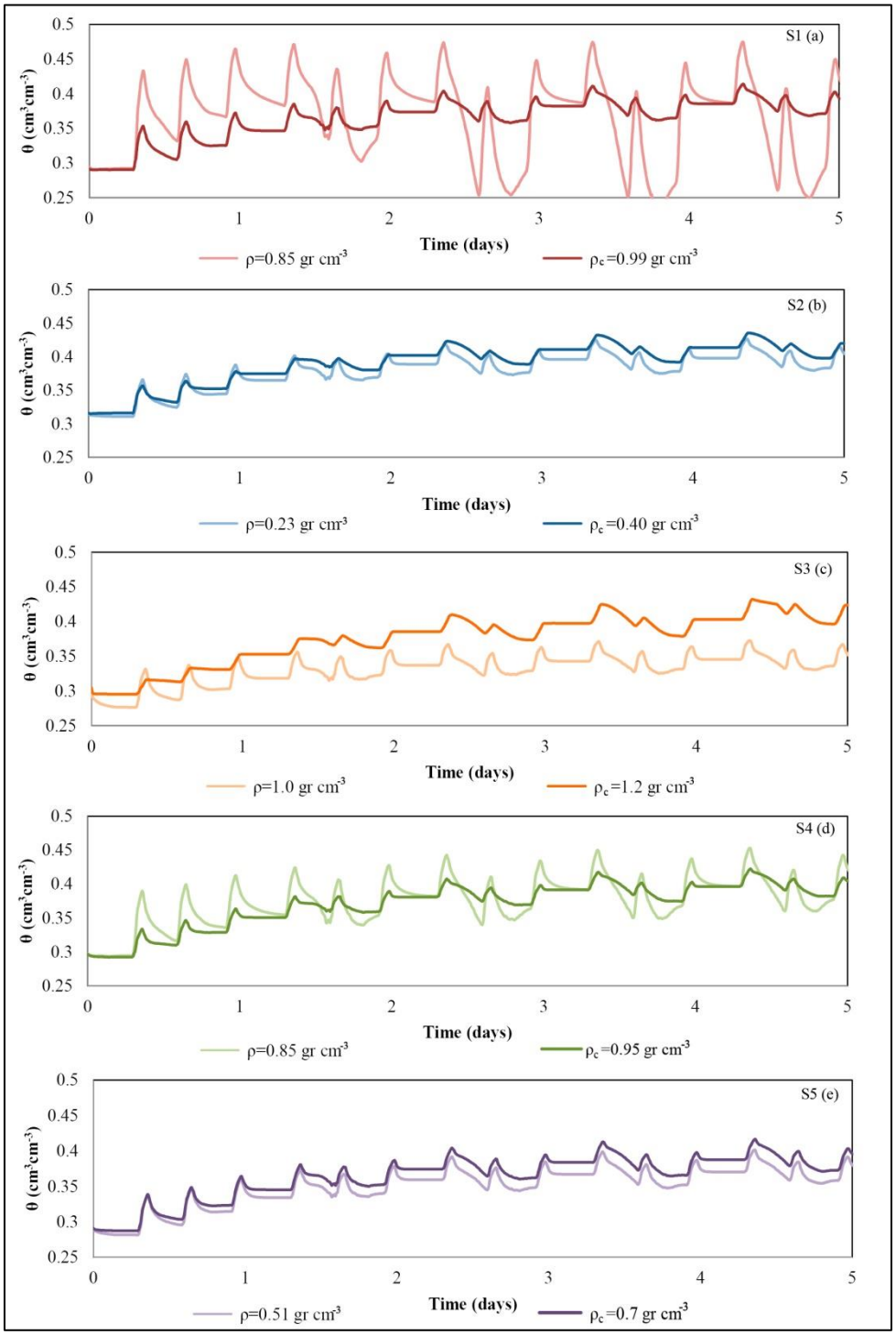

Figure 3-4: Modeled volumetric water content at the atmosphere-substrate interface. Light colors correspond to the uncompacted substrate, and dark compacted substrate. (a) substrate S1; (b) substrate S2; (c) substrate S3; (d) substrate S4; (e) substrate S5.

Figure 3-5 shows the cumulative water flux that exits from the bottom of each substrate throughout the simulations. Light colors correspond to the uncompacted substrate, and dark compacted substrate. The S2 substrate does not drain water during the simulations in either state, so it is not shown. It can be seen that the breakthrough time occurs earlier in the compacted substrates due to a reduction in the pore spaces. After compaction, the reduction in the breakthrough time of the substrates ranges between 1 h (S3) and 3 days (S4). In all the substrates the amount of water that drains the roof increases, especially in the S3 substrate where the cumulative water flux increases in more than 3 times. This significant increase in the cumulative water flux is the result of a decrease in the pore spaces and the changes in the response of each substrate to the atmospheric conditions.

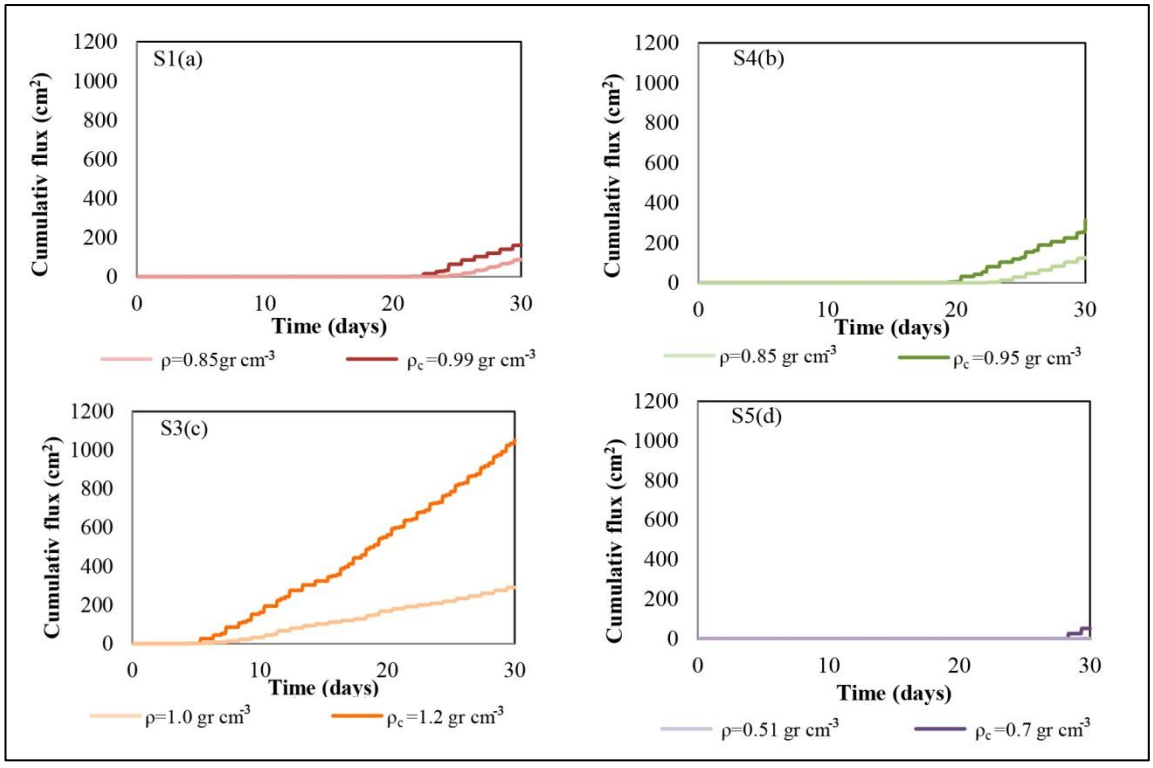

Figure 3-5: Cumulative flux that exits the bottom of the uncompacted (light lines) and compacted (dark lines) substrates during the 30 days of simulation. (a) substrate S1; (b) substrate S3; (c) substrate S4; (d) substrate S5. The results of the substrate S2 are not shown as this substrate did not drain water during the entire simulation.

Figure 3-6 shows the modeled temperature evolution of the five substrates in 30 days of simulation and at 34.5 cm below the surface, i.e., near the ceiling of the room. The changes at the roof ceiling when compaction occurs showed a general increment in the daily amplitude of the temperatures, which can be explained by the larger average water contents that can be seen in Figure 3-4 that provokes higher thermal conductivities and vertical heat diffusion. It can be seen that the change in temperatures at the ceiling due to compaction are mostly noticed in substrates S1 and S2. The temperature daily cycles of the uncompacted and compacted state is incremented in ~1°C in the case of S1 and S2. These changes in the thermal amplitude agree with the changes in the thermal conductivity curves shown in Figure 3-3.

Figure 3-7 shows the cumulative thermal energy (heating and cooling) consumed to mantain 23°C in the room below the roof system for the 30 days of simulation. It can be seen that the increment of the thermal daily amplitude, which is the result of substrate compaction, increases the heating and cooling energy due to natural convection. The biggest changes are related to substrates S1 and S2; in both cases the energy for heating gets reduced and the cooling energy increments. This behavior occurs due to the mixed effects of the general increment in thermal conductivity with moisture and the high porosity that reduces the vertical diffusion.

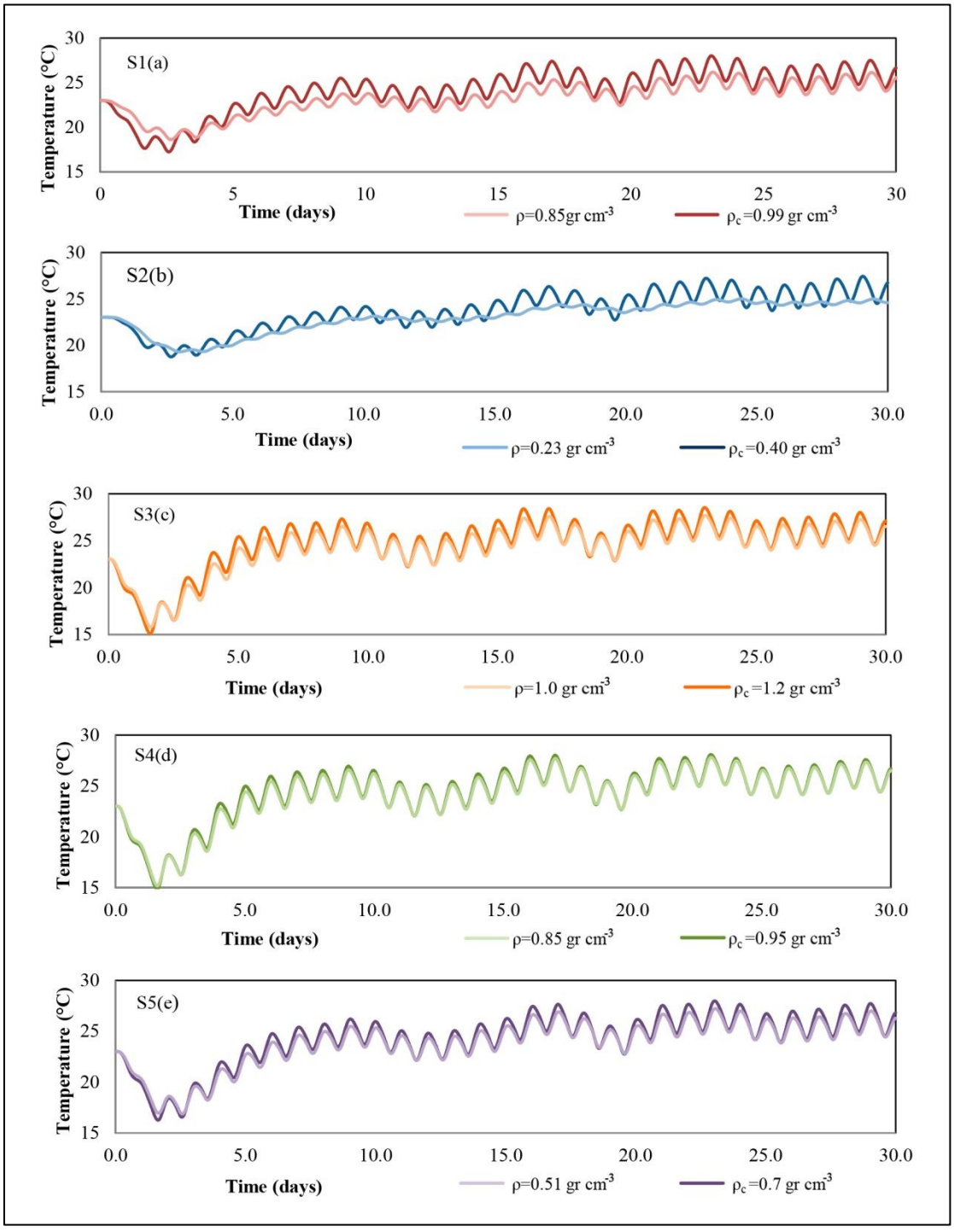

Figure 3-6: Modeled temperature evolution of the five substrates in 30 days of simulation and in 34.5 cm (concrete) below the surface. Light colors correspond to the uncompacted substrate, and dark compacted substrate.

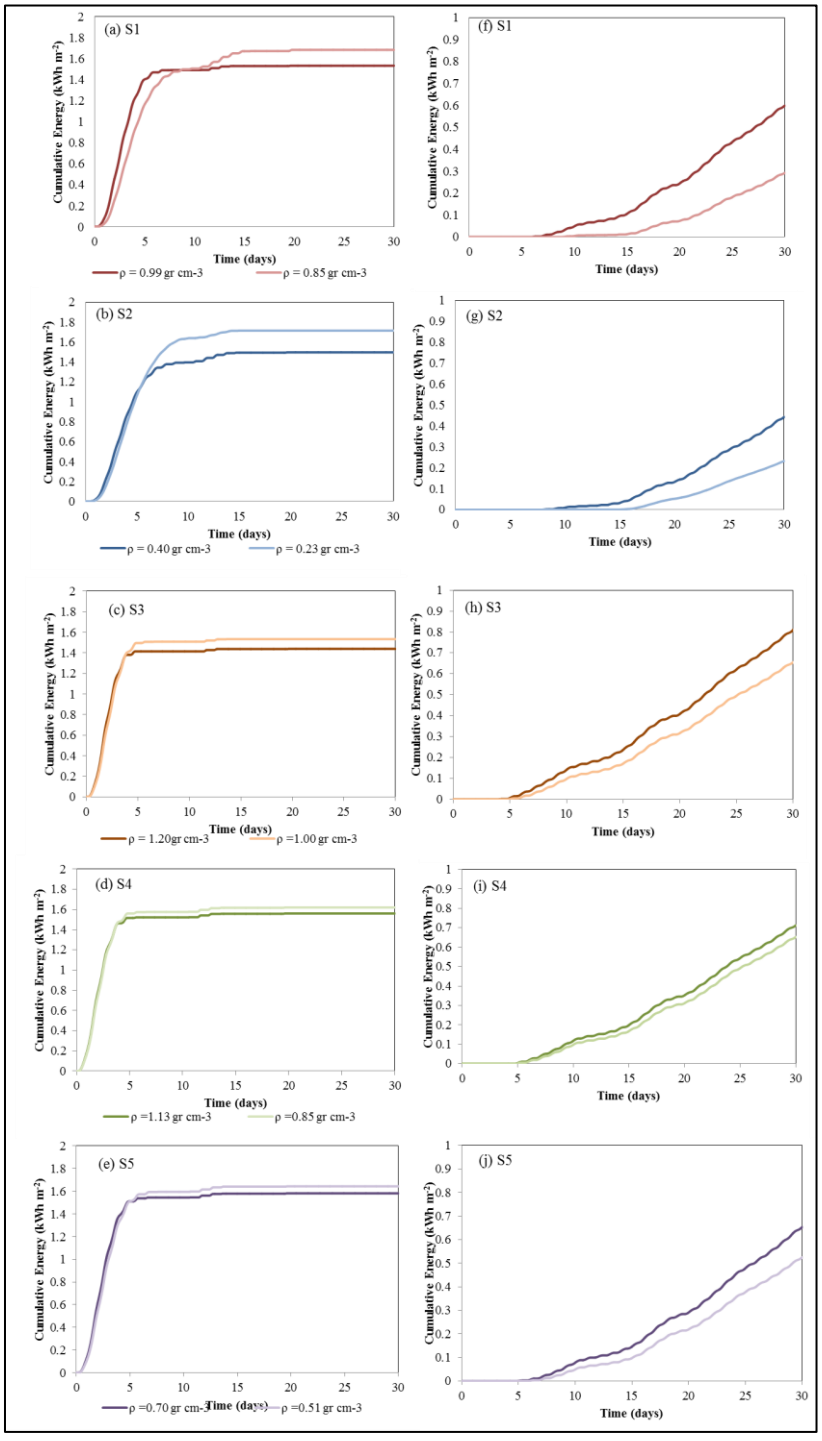

Figure 3-7: (a-e) Heating cumulative thermal energy required to maintain a reference room temperature of 23°C below the roof system. (f-j) Cooling cumulative thermal energy required to maintain a reference room temperature of 23°C below the roof system.

The comparison among the thermal conductivity curves of the five substrates in the uncompacted and compacted state –near to their maximum densities as shown in Table 3-1– can help understanding how the heat fluxes change through time in a green roof. Figure 3-3 shows that before compaction the substrates with higher thermal conductivity are S3 and S4. After compaction, the same pattern is observed, except when all the substrates are saturated. At this point, all the substrates reach thermal conductivity values of ~0.9 $Wm^{-1}K^{-1}$. In the case of the S2 substrate, the saturated thermal conductivity increases from 0.65 (uncompacted state) to 0.93 $Wm^{-1}K^{-1}$ (compacted state). In addition, the S2 substrate has the lowest thermal conductivity values for the entire range of moisture for both the uncompacted and compacted state. On the other hand, after compaction, the thermal conductivity of substrates S1 and S5 present similar values for the entire range of volumetric water content. The numerical simulations allow comparing the resulting thermal behavior of the substrates. It can be seen in Figure 3-7 that the energy required for heating and cooling for substrate S2 is smaller than that for substrates S1 and S5. Therefore, substrate S2 is more effective to reduce the vertical heat diffusion when compaction occurs. As explained in Chapter 2, the effect of the volumetric air content on the reduction of the heat diffusion is very important. In the simulations presented in this work, the S2 substrate presents a low average water content (i.e., the pore spaces have more air than water) since the substrate never reached saturation.

3.5 Conclusions

In this study, a new methodology to investigate how compaction affects the hydrodynamic and thermal properties of a porous medium was developed. This methodology was used to investigate the effects of compaction on the coupled water and heat transport in green roof substrates through numerical simulations. The results show that as the substrate is compacted, the pore-size of the substrates is reduced. As a result, the capillary forces increase and the water storage volume decreases. These results agree with other investigations performed in natural soils. However, because the foundations

of the new methodology are based on compaction methods developed for natural soils that have higher residual water contents and bulk densities compared to the artificial substrates, I observed that the new approach fails to produce reasonable results for some substrates. For instance, for substrates S3 and S4 the methodology predicts compacted residual water contents that are lower than those of the uncompacted state. For this reason, the proposed method can be used for green roof substrates that present residual volumetric water contents larger than 0.05 cm^3cm^{-3}.

Regarding the substrates thermal properties, the thermal conductivity curves increase their values as the bulk density increases. This increase in the thermal conductivity occurs because there is more physical contact between the solid particles of the media. The effect of compaction on the thermal conductivity curve was more relevant in the saturated part of the curves for all the substrates. Also, when considering that compaction also affects the hydrodynamic properties of the substrates, the variations of the thermal conductivity curve are now restricted to the new limits of moisture, which reduces the possible fluctuations of the thermal conductivity. Also, when the substrates have a very low bulk density (< 0.5 g cm^{-3}) the proposed method can present problems so care has to be taken when analyzing the results.

The numerical simulations showed that the water and thermal behaviors of the roof system change with compaction, reducing the amplitude of the fluctuations in the volumetric water content daily cycles, increasing the average water content and reducing the breakthrough time of the green roof substrates. When comparing the overall thermal behavior within the substrates studied, the S2 substrate reduces the vertical heat diffusion through the roof. Compaction changes the thermal behavior of the green roof substrates in different ways for each substrate due to the dependence of the air, water and soil fraction of each substrate.

The results showed that compaction affects the coupled water and heat fluxes in a hypothetical green roof. However, the compaction methodology needs an experimental validation for artificial substrates that have low bulk densities and residual water contents. Future research should focus on performing an appropriate experimental validation of this methodology to validate the results from the numerical simulations.

4 CONCLUSIONS AND PERSPECTIVES

In this study, the physical, hydrodynamic and thermal properties of five green roof substrates were determined experimentally and then used to understand their impact on the performance of a hypothetical roof system by means of numerical simulations. In all the substrates, the hydraulic response of the roof to the atmospheric forcing is strongly dependent on the substrate water retention characteristics. The heat transport trough the substrates strongly depends on the fraction of water, air and solid particles within the substrate, and the large water storage volume allows the attenuation of the diurnal thermal signal at the lowest boundary of the roof.

The compaction method results in a reduction of the pore spaces of the media that increase the substrate water retention and decrease its water storage volume. In the thermal conductivity curve, changes due to compaction shows different responses in each soil, increasing the overall conductivity. I found that the S2 substrate is the one with the best capacity to store water and to reduce storm-water runoff. It presents a low thermal conductivity and a large pore space, which results in low thermal conductivity values for dry conditions. The thermal behavior of the compacted substrates shows that the S2 substrate keeps having the smallest vertical diffusion of heat.

The simulation results showed that the behavior of the hypothetical roof system strongly depends on its hydrodynamic and thermal properties. Future work must be focused on studying the coupled heat and water fluxes due to the dependence of the hydrodynamic properties. The compaction method must be validated with experimental work.

The applications of the results of this investigation can be used to select appropriately a green roof substrate, and to optimize the configuration of these systems considering site-specific climatic conditions.

REFERENCES

Alaoui, A., Lipiec, J., and Gerke, H. H. (2011). A review of the changes in the soil pore system due to soil deformation: A hydrodynamic perspective. *Soil and Tillage Research*, *115–116*, 1–15. http://doi.org/10.1016/j.still.2011.06.002

Alfredo, K., Montalto, F., Asce, M., and Goldstein, A. (2010). Observed and Modeled Performances of Prototype Green Roof Test Plots Subjected to Simulated Low- and High-Intensity Precipitations in a Laboratory Experiment, *15 (6)*, 444–457. http://doi.org/10.1061/?ASCE?HE.1943-5584.0000135 CE

Aravena, J. E., Berli, M., Ruiz, S., Suárez, F., Ghezzehei, T. a., and Tyler, S. W. (2013). Quantifying coupled deformation and water flow in the rhizosphere using X-ray microtomography and numerical simulations. *Plant and Soil*. *376(1-2)*, 95-110.http://doi.org/10.1007/s11104-013-1946-z

Assouline, S. (2006a). Modeling the Relationship between Soil Bulk Density and the Water Retention Curve. *Vadose Zone Journal*, *5*(2), 554–563. http://doi.org/10.2136/vzj2005.0083

Assouline, S. (2006b). Modeling the relationship between soil bulk density and the hydraulic conductivity function. *Vadose Zone Journal*, *5(2)*, 697–705. http://doi.org/Doi 10.2136/Vzj2005.0084

Assouline, S., and Or, D. (2013). Conceptual and Parametric Representation of Soil Hydraulic Properties: A Review. *Vadose Zone Journal*, *12*(4). http://doi.org/10.2136/vzj2013.07.0121

Assouline, S., and Tartakovsky, D. M. (2001). Unsaturated hydraulic conductivity function based on a soil fragmentation process. *Water Resources Research*, *37*(5), 1309-1312.

Assouline, S., Tessier, D., and Bruand, A. (1998). A conceptual model of the soil water retention curve. *Water Resources Research, 34(2*), 223-231.doi:10.1029/97WR03039

ASTM D422-63, Standard Test Method for Particle-Size Analysis of Soils, Philadelphia: American Society for Testing and Materials, 2007.

ASTM D1557, Standard Test Methods for Laboratory Compaction Characteristics of Soil Using Modified Effort, Philadelphia: American Society for Testing and Materials, 2012.

Augeard, B., Bresson, L. M., Assouline, S., Kao, C., and Vauclin, M. (2008). Dynamics of Soil Surface Bulk Density: Role of Water Table Elevation and Rainfall Duration. *Soil*

Science Society of America Journal, *72*(2), 412–423. http://doi.org/10.2136/sssaj2006.0429

Balland, V., and Arp, P. A. (2005). Modeling soil thermal conductivities over a wide range of conditions. *Journal of Environmental Engineering and Science*, *4(6)*, 549–558. http://doi.org/10.1139/S05-007

Barry-Macaulay, D., Bouazza, A., Wang, B., and Singh, R. M. (2015). Evaluation of soil thermal conductivity models. *Canadian Geotechnical Journal*, *52*(11), 1892-1900.

Bristow, K. L., White, R. D., and Kluitenberg, G. J. (1994). Comparison of single and dual probes for measuring soil thermal properties with transient heating. *Soil Research, 32(3)*: 447-464.

Brunetti, G., Šimůnek, J., and Piro, P. (2016). A comprehensive analysis of the variably-saturated hydraulic behavior of a green roof in Mediterranean climate. *Vadose Zone Journal*, *15*. http://doi.org/doi: 10.2136/vzj2016.04.0032, (accepted June 15 2016)

Brown, C., and Lundholm, J. (2015). Microclimate and substrate depth influence green roof plant community dynamics. *Landscape and Urban Planning*, *143*, 134–142. http://doi.org/10.1016/j.landurbplan.2015.07.009

Brooks, R.H., and A.T. Corey. (1964). Hydraulic properties of porous media. *Hydrology. Paper no.3*. Colorado State Univ., Fort Collins

Buckland-Nicks, M., Heim, A., and Lundholm, J. (2016). Spatial environmental heterogeneity affects plant growth and thermal performance on a green roof. *The Science of the Total Environment*, *553*, 20–31. http://doi.org/10.1016/j.scitotenv.2016.02.063

Burszta-Adamiak, E., and Mrowiec, M. (2013). Modelling of green roofs' hydrologic performance using EPA's SWMM. *Water Science and Technology : A Journal of the International Association on Water Pollution Research*, *68 (1)*, 36–42. http://doi.org/10.2166/wst.2013.219

Camillo, P. J., and Gurney, R. J. (1986). A resistance parameter for bare-soil evaporation models. *Soil Science, 141(2)*: 95-105.

Causone F., Corgnati S.P., Filippi M., and Bjarne W.O (2009). Experimental evaluation of heat transfer coefficients between radiant ceiling and room. *Energy and Buildings, 41*: 622-628.

Campbell GS. (1985). *Soil physics with BASIC: Transport models for soil-plant systems*. Elsevier, New York.

Campbell GS, and Norman, J. (2013). *An introduction to environmental biophysics*. Springer, 2nd ed., New York.

Chung S-O, and Horton, R. (1987). Soil heat and water flow with a partial surface mulch. *Water Resources Research*, 23(12): 2175-2186.

Charpentier, S. (2015). Simulation of Water Regime and Sensible Heat Exchange Phenomena in Green Roof Substrates. *Vadose Zone Journal*, *14*(6), 1–9. http://doi.org/10.2136/vzj2014.07.0090

Côté, J., and Konrad, J. (2005). A generalized thermal conductivity model for soils and construction materials. *Canadian Geotechnical Journal*, *42*(2), 443–458. http://doi.org/10.1139/T04-106

Darcy, H. (1856). Les Fontaines Publiques de la Ville de Dijon, Dalmont, Paris.

DDC. (2007). Cool and Green Roofing Manual. Prepared for New York City Department of Design and Construction Office of Sustainable Design, by Gruzen Samton Architects LLP with Amis Inc. Flack and Kurtz Inc. Mathews Nielsen Landscape Architects P.C., and SHADE Consulting, LLC.

Fassman-beck, E., Asce, A. M., Wang, S., Simcock, R., and Liu, R. (2015). Assessing the Effects of Bioretention ' s Engineered Media Composition and Compaction on Hydraulic Conductivity and Water Holding Capacity. *J. Sustainable Water Built Environ.*, *1(4)*, 04015003 1-10. http://doi.org/10.1061/JSWBAY.0000799.

FLL. (2002). Guidelines for the planning, execution and upkeep of green-roof sites (*Forschungsgesellschaft Landschaftsentwicklung Landschaftsbau*, Bonn, Germany).

Getter, K. L., Rowe, D. B., Andresen, J. A., and Wichman, I. S. (2011). Seasonal heat flux properties of an extensive green roof in a Midwestern U.S. climate. *Energy and Buildings*, *43*(12), 3548–3557. http://doi.org/10.1016/j.enbuild.2011.09.018

Hashemi, S. S. G., Mahmud, H. Bin, and Ashraf, M. A. (2015). Performance of green roofs with respect to water quality and reduction of energy consumption in tropics: A review. *Renewable and Sustainable Energy Reviews*, *52*, 669–679. http://doi.org/10.1016/j.rser.2015.07.163

Hilten, R. N., Lawrence, T. M., and Tollner, E. W. (2008). Modeling stormwater runoff from green roofs with HYDRUS-1D. *Journal of Hydrology*, *358*(3–4), 288–293. http://doi.org/10.1016/j.jhydrol.2008.06.010

Jaffal, I., Ouldboukhitine, S.-E., and Belarbi, R. (2012). A comprehensive study of the impact of green roofs on building energy performance. *Renewable Energy*, *43*, 157–164. http://doi.org/10.1016/j.renene.2011.12.004

Johansen, O. (1975). Thermal conductivity of soils. Ph.D. thesis, University ofTrondheim, *CRREL Draft English Translation 637*, 1977.

Jury, W.A., and Horton, R. (2004). *Soil Physics*. John Wiley & Sons. 6th Edition, New Jersey.

Klute, A. (1994). *Methods of soil analysis, part 1: physical and mineralogical methods*. Agronomy Series, vol.9. American Society of Agronomy, Madison, Wisconsin.

Lamond, J. F., and Pielert, J. H. (2006). *Significance of tests and properties of concrete and concrete-making materials*. ASTM International, West Conshohocken, PA.

Li, Y., and Babcock Jr., R. W. (2015). Modeling Hydrologic Performance of a Green Roof System with HYDRUS-2D. *J. Environ. Eng., 141 (11)*, 04015036 1-9. http://doi.org/10.1061/(ASCE)EE.1943-7870.0000976.

Liu, R. and Fassman-Beck, E. (2016). Effect of Composition on Basic Properties of Engineered Media for Living Roofs and Bioretention. Journal of Hydrologic Engineering, 21(6): 06016002.

Metselaar, K. (2012). Water retention and evapotranspiration of green roofs and possible natural vegetation types. *Resources, Conservation and Recycling*, *64*, 49–55. http://doi.org/10.1016/j.resconrec.2011.12.009

Mualem, Y (1976). A new model for predicting the hydraulic conductivity of unsaturated porous media. *Water resources research*, 12(3): 513-522.

Palla, A., Gnecco, I., and Lanza, L. G. (2009). Unsaturated 2D modelling of subsurface water flow in the coarse-grained porous matrix of a green roof. *Journal of Hydrology*, *379*(1–2), 193–204. http://doi.org/10.1016/j.jhydrol.2009.10.008

Palla, a., Sansalone, J. J., Gnecco, I., and Lanza, L. G. (2011). Storm water infiltration in a monitored green roof for hydrologic restoration. *Water Science & Technology*, *64.3*(3), 766. http://doi.org/10.2166/wst.2011.171

Peng, L. L., and Jim, C. Y. (2015). Seasonal and Diurnal Thermal Performance of a Subtropical Extensive Green Roof: The Impacts of Background Weather Parameters. *Sustainability*, *7*(8), 11098–11113. http://doi.org/10.3390/su70811098

Peters, A., and Durner, W. (2006). Improved estimation of soil water retention characteristics from hydrostatic column experiments. *Water Resources Research, 42 (11)*, 1–9. http://doi.org/10.1029/2006WR004952

Philip, J.R., and de Vries, D.A., (1957) Moisture movement in porous materials under temperature gradient, *Eos, Transactions American Geophysical Union*, *38*(2), 222-232.

Pianella, A., Clarke, R. E., Williams, N. S. G., Chen, Z., and Aye, L. (2016). Steady-state and transient thermal measurements of green roof substrates. *Energy and Buildings*, *131*, 123–131. http://doi.org/10.1016/j.enbuild.2016.09.024

Pitt, R., and Clark, S (2008). Integrated Storm-Water Management for Watershed Sustainability. *Journal of Irrigation and Drainage Engineering, 134(5)*: 548-555.

Raimondo, F., Trifilò, P., Lo Gullo, M. A., Andri, S., Savi, T., and Nardini, A. (2015). Plant performance on Mediterranean green roofs: interaction of species-specific hydraulic strategies and substrate water relations. *AoB PLANTS*, *7*. http://doi.org/10.1093/aobpla/plv007

Raji, B., Tenpierik, M. J., and van den Dobbelsteen, A. (2015). The impact of greening systems on building energy performance: A literature review. *Renewable and Sustainable Energy Reviews*, *45*, 610–623. http://doi.org/10.1016/j.rser.2015.02.011

Rawls, W. J., Brakensiek, D. L., and Saxtonn, K. E. (1982). Estimation of soil water properties. *Transactions of the ASAE, 25(5)*: 1316-1320.

Reyes, R., Bustamante, W., Gironás, J., Pastén, P.A., Rojas, V., Suárez, F., Vera, S., Victorero, F., and Bonilla, C.A. (2016). Effect of substrate depth and roof layers on green roof temperature and water requirements in a semi-arid climate.*Ecological Engineering*, *97*, 624-632.

Richards, L.A. (1931) Capillary conduction of liquids through porous mediums, *Journal of Applied Physics*, 1(5): 318-333.

Saito, H., Simunek, J., and Mohanty, B. P. (2006). Numerical Analysis of Coupled Water, Vapor, and Heat Transport in the Vadose Zone. *Vadose Zone Journal*, *5*, 784–800. http://doi.org/10.2136/vzj2006.0007

Sailor, D. J. (2008). A green roof model for building energy simulation programs. *Energy and Buildings*, *40 (8)*, 1466–1478. http://doi.org/10.1016/j.enbuild.2008.02.001

Sailor, D. J., and Hagos, M. (2011). An updated and expanded set of thermal property data for green roof growing media. *Energy and Buildings*, *43 (9)*, 2298–2303. http://doi.org/10.1016/j.enbuild.2011.05.014

Sandoval, V.P., Suarez, F., Victorero, F., Bonilla, C., Gironás, J.A., Vera, S., Bustamante, W., Rojas, V., and Pasten, P. (2015). Impact of the Properties of a Green Roof Substrate on its Hydraulic and Thermal Behavior. *Energy Procedia*, 78: 1177-1182. http://doi.org/10.1016/j.egypro.2015.11.097

Schaap, M. G., and van Genuchten, M. T. (2006). A Modified Mualem–van Genuchten Formulation for Improved Description of the Hydraulic Conductivity Near Saturation. *Vadose Zone Journal*, *5(1),* 27. http://doi.org/10.2136/vzj2005.0005

Schindler, U. (1980): Ein Schnellverfahren zur Messung der Wasser-leitfähigkeit im teilgesättigten Boden an Stechzylinderproben. *Archiv fur Acker-und Pflanzenbau und Bodenkunde*. Berlin, *24*, 1–7.

Schneider, S., Mallants, D., and Jacques, D. (2012). Determining hydraulic properties of concrete and mortar by inverse modelling Sébastien. *Materials Research Society*, *1475*, 367–372. http://doi.org/10.1557/opl.2012. 601

Silva, C. M., Gomes, M. G., and Silva, M. (2016). Green roofs energy performance in Mediterranean climate. *Energy and Buildings*, *116*, 318–325. http://doi.org/10.1016/j.enbuild.2016.01.012

Šimůnek, J., Genuchten, M. T. van, and Šejna, M. (2008). Development and Applications of the HYDRUS and STANMOD Software Packages and Related Codes. *Vadose Zone Journal*, *7(2),* 587–600. http://doi.org/10.2136/vzj2007.0077

Simunek, J., Jacques, D., van Genuchten, M. T., and Mallants, D. (2006). Multicomponent geochemical transport modeling using HYDRUS-1D and HP1 (1). *Journal of the American Water Resources Association*, *42 (6)*, 1537–1547.

Šimůnek, J., van Genuchten, M. T., and Šejna, M. (2016). Recent Developments and Applications of the HYDRUS Computer Software Packages Developments. *Vadose Zone Journal*, *15(7)*. http://doi.org/10.2136/vzj2016.04.0033

Twarakavi, N. K. C., Šimůnek, J., and Schaap, M. G. (2010). Can texture-based classification optimally classify soils with respect to soil hydraulics? *Water Resources Research*, *46*(1), W01501 1-11. http://doi.org/10.1029/2009WR007939

U.S. DOE. (2016). EnergyPlus™ Version 8.6 Documentation: Engineering Reference. V-8.6 p. 165-175.

van Genuchten, M.Th. (1980). A closed-form equation for predicting the hydraulic conductivity of unsaturated soils. *Soil science society of America journal*, 44(5): 892-898.

Vera, S., Pinto, C., Victorero, F., Bustamante, W., Bonilla, C., Gironás, J., and Rojas, V. (2015). Influence of plant and substrate characteristics of vegetated roofs on a supermarket energy performance located in a semiarid climate. *Energy Procedia*, *78*, 1171–1176. http://doi.org/10.1016/j.egypro.2015.11.089

Vijayaraghavan, K. (2016). Green roofs: A critical review on the role of components, benefits, limitations and trends. *Renewable and Sustainable Energy Reviews*, *57*, 740–752. http://doi.org/10.1016/j.rser.2015.12.119

Yaghoobian, N., and Srebric, J. (2015). Influence of plant coverage on the total green roof energy balance and building energy consumption. *Energy and Buildings*, *103*, 1–13. http://doi.org/10.1016/j.enbuild.2015.05.052

Zhao, M., Tabares-Velasco, P. C., Srebric, J., Komarneni, S., and Berghage, R. (2014). Effects of plant and substrate selection on thermal performance of green roofs during the summer. *Building and Environment*. http://doi.org/10.1016/j.buildenv.2014.02.011

Zhou, A.-N., Sheng, D., and Carter, J. P. (2012). Modelling the effect of initial density on soil - water characteristic curves. *Geotechnique*, *62*(8), 669–680. http://doi.org/10.1680/geot.10.P.120